



LAWRENCE
LIVERMORE
NATIONAL
LABORATORY

Analyses in Support of Z-IFE LLNL Progress Report for FY-05

R. W. Moir, R. P. Abbott, D. A. Callahan, J. F.
Latkowski, W. R. Meier, S. Reyes

October 19, 2005

Disclaimer

This document was prepared as an account of work sponsored by an agency of the United States Government. Neither the United States Government nor the University of California nor any of their employees, makes any warranty, express or implied, or assumes any legal liability or responsibility for the accuracy, completeness, or usefulness of any information, apparatus, product, or process disclosed, or represents that its use would not infringe privately owned rights. Reference herein to any specific commercial product, process, or service by trade name, trademark, manufacturer, or otherwise, does not necessarily constitute or imply its endorsement, recommendation, or favoring by the United States Government or the University of California. The views and opinions of authors expressed herein do not necessarily state or reflect those of the United States Government or the University of California, and shall not be used for advertising or product endorsement purposes.

This work was performed under the auspices of the U.S. Department of Energy by University of California, Lawrence Livermore National Laboratory under Contract W-7405-Eng-48.

Analyses in Support of Z-IFE

LLNL Progress Report for FY-05

**R.W. Moir, R.P. Abbott, D.A. Callahan,
J.F. Latkowski, W.R. Meier, S. Reyes**

September 30, 2005

This work was performed under the auspices of the U.S. Department of Energy by University of California, Lawrence Livermore National Laboratory under Contract W-7405-ENG-48.

Contents

1. Summary.....	1
2. Introduction.....	3
3. Proposed Design Features, Analyses and Special Topics.....	5
3.1 Frangible Flibe RTL as an Alternative to Steel RTL.....	5
3.2 Carbon Composite Chamber Material as an Alternative to Steel.....	6
3.3 Systems Studies – Advantages of High Yield and Rep-Rate	7
3.4 Dynamic Insertion of RTL – Approach and Advantages	9
3.5 Chamber Design and Liquid Flow Shielding.....	10
3.6 Primary Loop Description.....	15
3.7 Pumping Power.....	16
3.8 Chamber with Minimal Gas Pressure as Alternative to ~20 Torr of Inert Gas	19
3.9 Tritium Recovery System and Tritium Inventory.....	19
3.10 Neutronics – Direct Conversion from CAD to Monte Carlo.....	20
3.11 Choice of High-Z Material - Advantages and Disadvantages of Hg, Pb and W	22
3.12 Flibe Cleanup and High-Z Material Recovery for Recycle.....	26
3.13 Thermal Stress in Chamber Walls	27
3.14 Output from Z-IFE Targets.....	27
4. Findings and Recommendations.....	31
Appendices with Additional Detail.....	33
A.1 Thermal Stress During Insertion and Casting of RTL.....	33
A.2 Tritium Inventory in Z-IFE Carbon Composite Chamber Walls.....	39
A.3 Flibe Vapor Pressure and Evaporation (Condensation) Rates.....	42
A.4 Flibe Processing.....	44
A.5 Flat Plate Heat Exchanger Based on Carbon Composites with Sic Barriers	45
A.6 Thermal Stress in Carbon-Carbon (C-C) First Wall.....	52

1. Summary

The FY04 LLNL study of Z-IFE [1] proposed and evaluated a design that deviated from SNL's previous baseline design. The FY04 study included analyses of shock mitigation, stress in the first wall, neutronics and systems studies. In FY05, the subject of this report, we build on our work and the theme of last year. Our emphasis continues to be on alternatives that hold promise of considerable improvements in design and economics compared to the base-line design. Our key results are summarized here.

1.1 Key Design Features

Frangible Flibe RTL

We have evaluated the design of a recyclable transmission line (RTL) made of flibe rather than steel. Parts of the RTL that are not completely vaporized by the fusion yield are designed to shatter into small pieces (like windshield glass), i.e., designed to be frangible. Replacing the steel RTL with a frangible flibe RTL eliminates the steel recovery and fabrication plant part of the power plant that has been estimated in the region of \$1B capital cost.

Dynamic Insertion of RTL

By using dynamic RTL insertion, we can keep the g-loadings below 2 g's and achieve pulse rates of > 0.5 Hz. Dynamic insertion aids neutron shielding of the sensitive components such as the magnetic insulated transmission line (MITL) and mitigates shocks by downward momentum of a 10 m/s slug of flibe.

Carbon Composite Chamber Material, High Operating Temperature

The use of carbon composites as an alternative to steel allows operation at ~1100 °C where hydrogen production and a high efficiency Brayton power conversion cycle become attractive.

Low Background Pressure of Non-condensable Gas (<10⁻⁵ Torr)

A low base pressure in the chamber eases the problem of maintaining low gas pressure in the RTL and MITL and eases tritium recovery.

Higher Yield, Higher Pulse Rate

Our design is for 4.6 GJ rather than the 3 GJ nominal yield of the base-line design, and we propose a pulse rate of 0.5 Hz rather than 0.1 Hz. We also propose that the plant consist of fewer chambers, perhaps one or two depending on the desired total plant power, since economies of scale push toward fewer larger chambers.

1.2 Summary of Analyses

The proposed design features of course give rise to many issues that need R&D to demonstrate their feasibility. This report documents our analyses to begin addressing these issues. We have included proposed procedures for fabrication of the flibe RTL and analyses of thermal stresses during casting and insertion. We describe a dynamic insertion method and present analyses of relevant parameters and mechanical loads. Issues related to tritium recovery and tritium hold-up in the carbon composite structures are discussed and evaluated. The choice

of the high-Z target material will impact the chamber and plant operation; we briefly discuss the advantages and issues of several candidates (W, Pb, Hg). We continued our neutronics work with a focus on testing an automated CAD to Monte Carlo conversion tool and applying it to the new LLNL chamber concept. By its nature, systems modeling lags the design progress, so significant improvements will be coming in the next FY as this year's information is included. We did however make minor updates and include an analysis showing the benefits of high yield and pulse rate. We also completed a target burn calculation for a Z-IFE target design and used the output spectrum information to make a preliminary evaluation of the idea of directed energy output as previously proposed by Dr. Per Peterson at UC Berkeley.

1.3 Summary of Recommendations

Although we have made good progress on this alternative design concept, in most cases more detail design and analyses, significant development, experiments on specific phenomenon, and proof of concept experiments will be required. Specifically we recommend the following:

Flibe RTL

Significant work is needed to address key issues associated with the use of flibe for the RTL, but the benefits are so compelling that development should be given high priority within the Z-IFE program. Proposed work includes:

- Experiments to investigate methods of producing frangible flibe RTLs, including casting in carbon composite molds as suggested here.
- Experiments to simulate the mechanical loads and response of the RTL (e.g., maintaining the gap tolerance between inner and outer cones during dynamic insertion). Include the investigation of the ability to make adequate electric contact during dynamic insertion.
- Further analyses and experiments on the plasma conductivity of flibe RTL and ability to handle the required currents. Include evaluation of need for a conducting coating to assist in "turn-on".
- Integrated optimization of the RTL design considering mechanical and nuclear as well as electrical performance to achieve long component life, low cost of the pulse power system and good overall economics.

Carbon Composite Structure

One of the key concerns with respect to the use of carbon composites is limiting the amount of tritium that is trapped and the resultant tritium inventory. Recommendations include:

- Material development to demonstrate the ability to embed a thin SiC layer to form a tritium barrier.
- Tests to evaluate the effectiveness of the proposed SiC layer as a permeation barrier, including possible degradation due to cracking resulting from pulsed mechanical loading and radiation damage..

2. Introduction

The LLNL team benefits from 25 years of experience on similar studies, including HYLIFE-I, HYLIFE-II and CT inertial fusion power plants [1-4]. The yields (up to 4.8 GJ) considered in these designs exceeded the baseline Z yield. The HYLIFE-CT, a compact torus accelerator design used a frangible flibe recyclable transmission line. The work reported here reflects the fact that our statement of work gave us the flexibility and directive to look at alternatives to the Sandia baseline design, which features steel RTLs, ten steel chambers, 0.1 Hz pulse rate and RTL/MITL transition region on top of the chamber that has minimal shielding from neutrons.

Our first design of an RTL plus its insertion equipment achieved good neutron shielding and good shock mitigation and a cycle time of 1.6 s (0.6 Hz) with a maximum of 2 g's acceleration on the RTL. However its inductance was high (>25 nH) resulting in an uncomfortably large pulsed power system. We have reduced the inductance by half and now better understand the trade-offs involved between inductance (size of the pulsed power system) and neutron management (shielding and shock mitigation). The key insight is to use dynamic insertion for rapid cycle time but more importantly for shock mitigation at the top. The falling RTL with a downward velocity of ~10 m/s has substantial downward momentum (20,000 P·s) that can overwhelm the upward impulse from the explosion.

We choose to operate with a background pressure of non-condensable gases of less than 10^{-5} Torr as opposed to the baseline design of 20 Torr of inert gas. Low pressure allows cryogenic pumping of tritium and ease of maintaining the $<10^{-5}$ Torr in between the inner and outer cones of the RTL required for power transmission. High pressure (20 Torr) poses a difficult tritium removal problem and poses difficult design problems for the RTL.

Section 3 of this report documents the proposed design features, supporting analyses, and special topics. In some cases, additional detail is given in the Appendices. Section 4 covers our findings and recommendations. Table 2.1 gives some key features of the proposed design.

Table 2.1 Features of LLNL's Proposed Z-IFE Design

Chamber material	Carbon Composite
RTL material	Flibe
Yield	4600 MJ
Rep-rate	0.5 Hz
Fusion power	2300 MWt
Thermal power	2645 MWt
Flibe outlet temperature	1100 C
Conversion efficiency	~50%
Gross electric power	1323 MWe
Chamber inner radius, m	5
Chamber height, m (nozzle to bottom collection region)	8

References for Section 2

- [1] J.A. Blink, W.J. Hogan, J. Hovingh, W.R. Meier, and J.H. Pitts, “The high-yield lithium-injection fusion-energy (HYLIFE) reactor,” UCRL-53559 (1985).
- [2] R.W. Moir, R.L. Bieri, X.M. Chen, T.J. Dolan, M.A. Hoffman, P.A. House, R.L. Leber, J.D. Lee, Y.T. Lee, J.C. Liu, G.R. Longhurst, W.R. Meier, P.F. Peterson, R.W. Petzoldt, V.E. Schrock, M.T. Tobin, W.H. Williams, “HYLIFE-II: A Molten Salt Inertial Fusion Energy Power Plant Design-Final Report,” *Fusion Technology*, **25**, 5-25 (1994).
- [3] B.G. Logan, R.W. Moir, M. Tabak, R.L. Bieri, J.H. Hammer, C.W. Hartman, M.A. Hoffman, R. L. Leber, R. W. Petzoldt, M. T. Tobin, “Compact Torus Accelerator Driven Inertial Confinement Fusion Power Plant HYLIFE-CT,” UCRL-TR-211025 (2005).
<http://www.osti.gov/servlets/purl/15016028-yK40cw/native/>
- [4] R.W. Moir, J.H. Hammer, C.W. Hartman, R.L. Leber, B.G. Logan, R.W. Petzoldt, M.Tabak, and M.T. Tobin, “Inertial Fusion Energy Power Plant Design Using the Compact Torus Accelerator: HYLIFE-CT,” *Fusion Technology*, **21** 1492 (1992).

3. Proposed Design Features, Analyses and Special Topics

In this section of the report we describe key features the proposed alternative RTL and chamber design, cover the analyses to address key issues, and discuss several special topics. Additional details are given in appendices.

3.1 Frangible Flibe RTL as an Alternative to Steel RTL

The advantage of frozen flibe for the RTL is that once used the debris becomes indistinguishable from the coolant. Recycle is automatic. The broken pieces must melt before they cause damage to hardware such as pump impellers. By contrast, iron RTL material will come in various forms: condensed vapor, condensed droplets, and shrapnel in various sizes (up to a fraction of a meter for the material near the top of the RTL furthest away from the microexplosion and 2 m long for duds). This will require a filtration system that can be avoided if the frozen flibe alternative is plausible. Also the recovered iron must be fabricated in an iron mill for new RTLs.

Will a flibe RTL work from an electrical point of view? Experiments [1] with iron and mylar mock-up transmission lines showed that iron delivered more of its power to the target, particularly in the early period of the pulse. However, later in the pulse the plasma on the surface carried the current and both deliver about the same power. The researchers concluded mylar was not ruled out, although iron was preferred from a power delivery efficiency point of view. Based on this conclusion we assume flibe, whose conductivity is also low like mylar, will work albeit with some power loss. A conductive coating placed on a flibe RTL might recover some of the losses.

Replacing the steel RTL baseline design with an alternative design of a frangible flibe RTL will eliminate the steel recovery and fabrication plant part of the power plant that has been estimated in the region of \$1B capital cost. Frangible means designed to be breakable or shatter in the same way automobile windshields are made to fail by shattering into small pieces for safety reasons. The question that comes up is: "Does the surface of the frozen transmission line need to have its conductivity enhanced by adding coatings?" This is a research item whose outcome will determine the feasibility of the idea of using frozen frangible flibe for the RTL. Another question is the possibility of premature shattering during insertion into the hot flibe vapor. Experiments will be needed to see if this is indeed a serious feasibility issue. Could the glassy nature of some frozen salt phases relieve stresses enough to avoid or prolong the shattering? Are there surface conditioning processes that could make the RTL more shatter resistant? Are there protective thermal layers possible such as injecting a cooler flibe layer on the RTL during insertion? The shattering hazard could be resolved with some low cost experiments and is discussed more fully in Appendix A.1.

3.2 Carbon Composite Chamber Material as an Alternative to Steel

The baseline design calls for a steel chamber. This limits the temperature to about 600 °C depending on the alloy used. If carbon composites could be used, the temperature could be much higher. Working temperatures in excess of 1100 °C appear possible. The advantage would be the ability to deliver heat at the temperatures a Brayton cycle would operate at with high efficiency. The power density will also be higher so that the equipment might be lower cost than for a steam cycle. Another use is to deliver heat to a hydrogen production facility either based on thermochemical cycles or high temperature electrolysis. Flibe is compatible with carbon composites.

The Sombrero design [2] chose carbon composites about 15 years ago. At the present state of the art of carbon composites it would be not be feasible to build the Z-IFE chamber out of this material. However, this technology is rapidly evolving, and we can speculate that the outcome might change especially with the work going on in other programs. Therefore we are looking at a carbon composite chamber as an alternative to the steel baseline design. Carbon is compatible with flibe in the sense of nil corrosion. The stress allowed in carbon composites is independent of temperature up to 2000 °C or so. A challenge will be the vapor pressure from the flibe itself will get into the few Torr range.

Past safety work for the Sombrero design showed that oxidation of the carbon-based chamber structures might occur under loss-of-vacuum accident scenarios [3]. Due to potential tritium retention in carbon structures, oxidation prevention is key to minimize radioactivity release in case of an accident. In order to address SOMBRERO safety concerns, a series of Carbon Fiber Composites (CFC) combustion tests were performed at Idaho National Laboratory (INL) that provided new data on C/C oxidation [4]. Such new data suggested that partial oxidation of C/C chamber structures might happen during an air ingress event, and that material choice is critical in order to minimize the reaction rates. In order to prevent the oxidation of chamber structures in Z-IFE, safety features should be implemented such as SiC coatings in outer chamber structures and/or first wall, and passive chamber flooding with an inert gas such as CO₂.

Some of the research items for carbon composites will be how to seal against gas leaks, especially tritium. One possibility is the use of SiC barriers built into the interior of the composites. Another issue is how to make joints. Another is the piping and heat exchanger must also be made of carbon composites; here we suggest the flat plate heat exchanger concept discussed in Appendix A.5.

The thermal stress for a 0.1 m thick C-C wall cooled with internal coolant channels was found to be low (0.2 MPa, see details in Appendix A.6). This low stress is due to the good thermal properties of C-C and to the strong neutron attenuation of a 1-m equivalent thick layer of flibe jets.

The design of the chamber can be of the pool type as in the baseline design or the loop type. Use of carbon composites or steel probably does not determine which type is used. The pool type avoids erosion issues some by slowing down the high-speed jets in the pool. A disadvantage is splashing because there is little or no mechanism to dissipate energy in the falling liquid jets,

hence we expected considerable splashing so the inter-pulse time will have to be longer with the pool type to allow splashing to settle down and gravity to clear the chamber. The loop type as used in HYLIFE-II mitigates the splash problem by directing the downward motion into a deflector that makes the motion rotate in the torus below the chamber. This directed motion in addition to reducing splashing allows recovery of about half of the kinetic energy of the liquid and thereby reduces pumping power.

Due to the high temperature of 1100 °C not only the chamber but also the piping and heat exchanger to a secondary liquid will need to be made of carbon composites. This brings up the issue of joining and gas tight barrier including tritium in the heat exchanger and piping.

A unique feature of carbon composites is its affinity to hold onto tritium. As in the Sombrero design we found the tritium inventory was acceptable. This is discussed in Section 3.9 and Appendix A.2.

3.3 Systems Studies – Advantages of High Yield and Rep-Rate

Progress on the systems modeling depends on development of more detailed designs and understanding of the major subsystems of the Z-IFE power plant. The Z-IFE project is still in an early exploratory phase evaluating a variety of target, pulsed power, RTL, and chamber options and configurations that can have significant impact on the economic attractiveness of the integrated power plant. While it is too early in the process to develop a credible integrated systems model, the group has developed better understanding of some key trade-offs. These include

- More detailed analyses of various target options (double-ended hohlraum, dynamic hohlraum, etc.) have given a better idea of the drive conditions and energy require for high yield. Based on results presented near the end of this FY, the dynamic hohlraum appears to have the best performance with 42 MJ delivered to the pinch giving a yield of 4.6 GJ. This is 4-5 times less drive energy than the double-ended hohlraum for comparable yields.
- Driver efficiency is a key consideration for any IFE power plant. For Z-IFE, pulsed power alternatives are being compared based on their efficiency from wall-plug electrical input to energy delivered to the target. At this point, the linear transformer driver (LTD) technology is a clear choice with an efficiency of 40-60% compared to <20% for Z technology.
- Choice of the RTL design will have a significant economic impact; SNL estimated the cost of a steel RTL processing plant at ~\$1B. This puts added emphasis on finding a viable alternative such as cast flibe as proposed here.
- Little additional information has come available on driver cost, but again, this could have a large impact. A low cost for the driver system has long been claimed as an advantage of Z-IFE; this must be validated.

Based on our preliminary work last year, we still believe that pushing Z power plant concept in the direction of highest possible yield and pulse rate per chamber is advantageous. Building ten separate pulsed power systems to drive ten 3-GJ, 0.1-Hz chambers will almost certainly be a

non-starter. As described throughout our report, we are pushing to higher yields (4.6 GJ), higher pulse rates (0.5 Hz), and higher operating temperatures (1100 °C), all of which will help the economics of Z-IFE if the significant development challenges can be successfully met.

Figure 3.3.1 illustrates the point. It shows the normalized cost of electricity (COE) as a function of rep-rate for two yields, 3.0 GJ and 4.6 GJ (our base case). These results are based on the crude systems model documented in last’s year’s progress report but updated with two changes: the driver efficiency is 50% based on the use of LTDs, and the target gain curve scales as $E^{2/3}$ from the 4.6 GJ yield design with 42 MJ delivered to pinch. Figure 3.3.1 assumes a single chamber for the power plant. The COE is normalized to the 4.6 GJ, 0.5 Hz result, which corresponds to ~1.2 GWe net power. Increasing rep-rate from 0.1 to 0.5 Hz reduces the COE by >50% for both targets. At a given rep-rate, the 4.6 GJ yield has a ~14% advantage. Also shown are two constant net power levels, 0.6 GWe (circles) and 1.2 GWe (diamonds). For fixed net power, the higher yield target give a COE that is only slightly lower, but the required pulse rate is less.

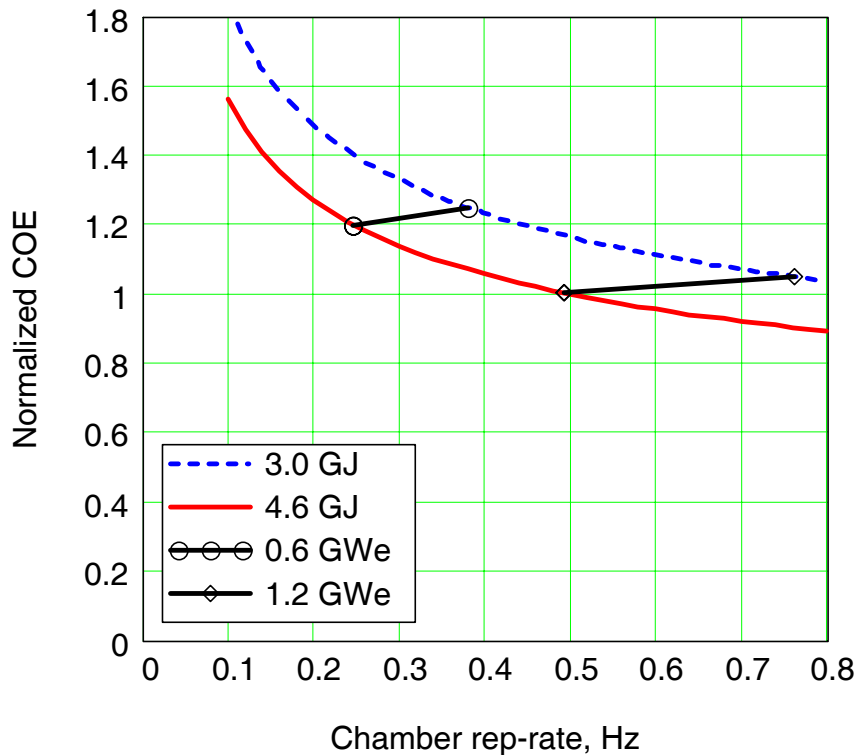


Fig. 3.3.1. Normalized COE as a function of rep-rate for fixed target yield (3.0 and 4.6 GJ) and for fixed net power (0.6 and 1.2 GWe).

3.4 Dynamic Insertion of RTLs – Approach and Advantages

The key insight is to use dynamic insertion for rapid cycle time but more importantly for shock mitigation at the top. The RTL, which is moving downward at ~ 10 m/s, amounts to a substantial downward momentum ($20,000$ P·s) that may dominate over the upward impulse from the target. In a very preliminary time-and-motion study we found a 1.6 s cycle time with a 2 g maximum loading on the RTL in the sideways direction. During insertion the RTL experiences guided free fall during about 1 s of travel time. A critical issue is the sufficiency of the electrical contact of the RTL with the MITL as it slides by at about 10 m/s.

The Fig. 3.4.1 shows the RTL holder attached to the RTL just before it passes by the face of the MITL electrodes. The sleeve intended to cover the MITL face to prevent gas from entering is shown withdrawn. As the RTL slides over the MITL surface, the pulse power sends current to the target via the RTL.

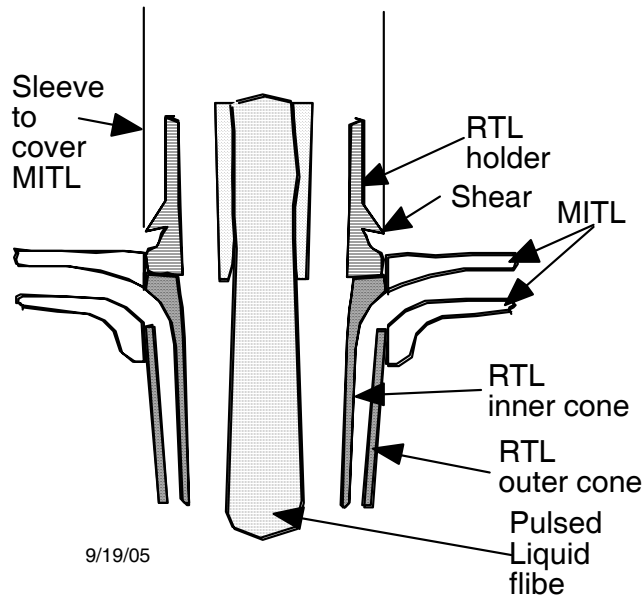


Fig. 3.4.1. The components near the RTL interface with the MITL are shown at shot time.

In Fig. 3.4.2 the components are shown after the shot where the RTL has been shattered. The RTL holder with its shear passes the MITL face, cleaning it off. The sleeve moves in place to cover the MITL face to protect it from gas entering.

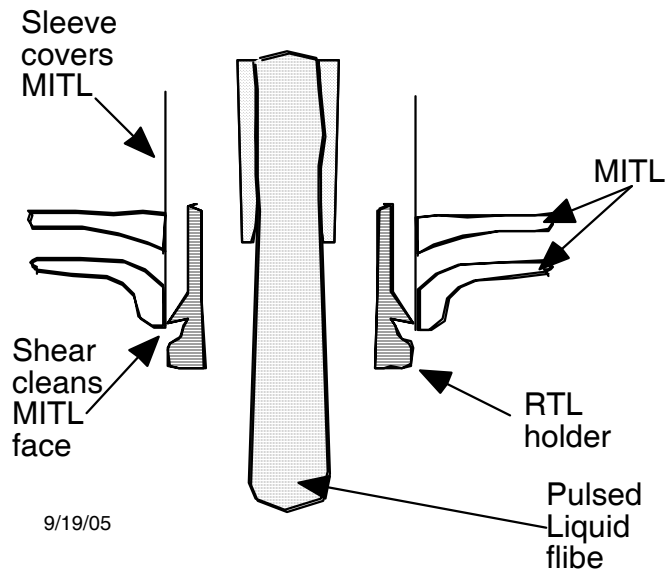


Fig. 3.4.2. The components near the RTL interface with the MITL are shown shortly after shot time.

3.5 Chamber Design and Liquid Flow Shielding

3.5.1 Introduction

A refinement of the FY04 LLNL Z-IFE chamber design concept has been carried out in an effort to reduce pumping power requirements, simplify construction and maintenance, and mitigate the threat of damage from coolant hydraulic response. The design assumes a power plant built around a single fusion chamber pulsed at a relatively high rep-rate of 0.5 Hz and employing targets with yields of 4.6 GJ. To allow for higher operating temperatures and thermodynamic efficiencies, carbon-carbon (C-C) composite is used for the first structural wall (FSW) and all other coolant contacting structures. Some of the dramatic deviations from the baseline Z-IFE chamber include: the elimination of the static pool below the target, use of a kinetic head recovery system for the shielding flow, implementation of recyclable transmission lines (RTL's) made from frangible flibe, a shield curtain geometry that improves pocket venting, and a divergent FSW profile that reduces liquid impact stresses.

Much of the design work has been carried out using computer aided modeling, the most significant component being the construction of an integrated parametric CAD model of the chamber. This approach has yielded several advantages, the most obvious being the ability to quickly modify various design parameters as new ideas and analysis improve our understanding of the engineering challenges faced. Other benefits have included leveraging of new technology allowing the direct conversion of the CAD model to Monte Carlo neutron transport codes such as TART and MCNP. Figure 3.5.1 illustrates this.

The following sections lay out the main qualitative features of the chamber design and the considerations that led to its current form. Most of these are oriented around the goal of reducing the number of fusion chambers needed to achieve a given electric power output. Fewer chambers require fewer pulsed power systems, a smaller flibe inventory, lower pumping power requirements, lower construction and waste disposal costs, and a much more simplified and attractive plant configuration. All of these advantages lead to yet another: a lower cost of electricity.

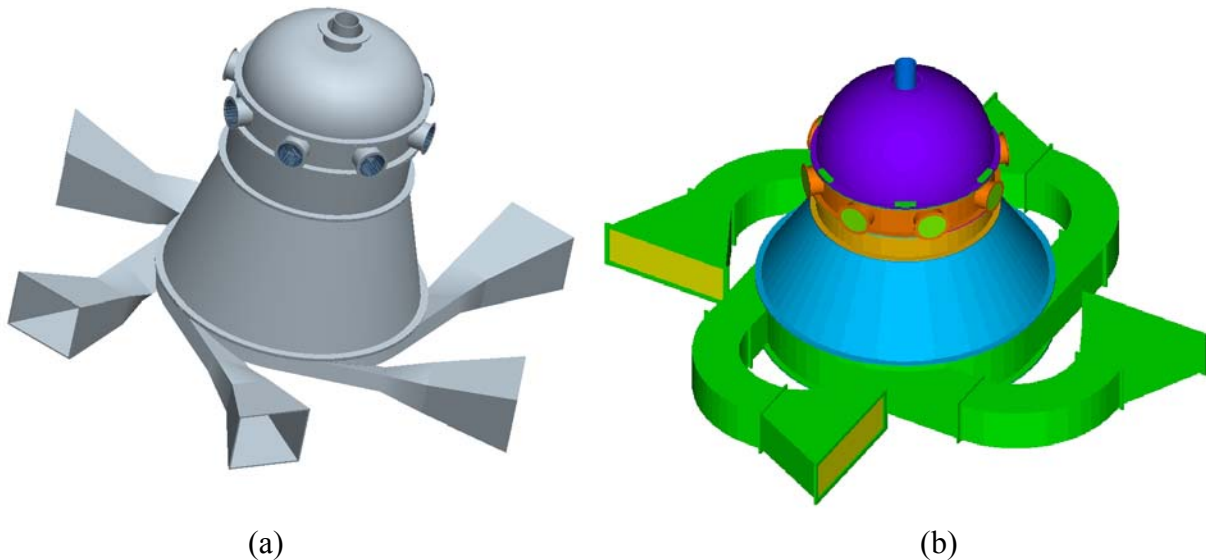


Fig. 3.5.1. (a) LLNL's FY05 Z-IFE fusion chamber CAD model and (b) the direct conversion of an earlier version to a TART neutronics model.

3.5.2 Structural Material Selection

Carbon-carbon (C-C) composite presents several advantages over more traditionally selected chamber materials. The most important of these is its high operational temperature limit. While chambers designed using steel must keep their coolant temperatures below about 650 °C, a chamber built of C-C composite could operate with some margin using coolant temperatures of 1100 °C. This allows for significantly increased thermodynamic conversion efficiencies, the main benefit of which is to reduce the number of chambers at a given yield and repetition rate needed for a given net electric power output. There would be potentially valuable auxiliary uses for these high temperatures as well such as electrolysis or iodine-sulfur hydrogen production.

C-C composite also has superior thermal conduction properties to many other materials. This allows for the design of chambers with greater power densities (increased repetition rates and/or target yields) by keeping thermal stresses and the need for actively cooled chamber structures to a minimum. Once again, this helps reduce the total number of chambers needed for a given net electric power output.

One disadvantage C-C composite has is that it swells at relatively low neutron damage regimes, which necessitates the use of a greater amount of flibe for neutron shielding at a given chamber power density. Fortunately, since neutron intensity drops off exponentially with shield

layer thickness, adequate shielding does not require flibe flow rates to go up nearly as quickly as power density can. These and other advantages of C-C composites are discussed in more detail in other sections of this report. Before C-C composites become an acceptable construction material, solutions for preventing gas leakage, joining and repair must be demonstrated.

While the chamber material choice affects the nature of the thermal stresses that will arise, its shape plays an important role in what mechanical stresses it will experience from the large shielding liquid disruptions. It was shown in LLNL's FY04 report that bulks liquid motion resulting from a fusion pulse could cause significant mechanical stresses in the FSW were the liquid to stagnate against it. The FY05 chamber design, therefore, incorporates a divergent wall profile such that liquid is nominally expected to miss the FSW entirely as it follows a conical trajectory dictated by its axial and induced radial motion to the impeller blades at the bottom.

3.5.3 Thick-Liquid Neutron Shielding Configuration

The FY05 LLNL Z-IFE chamber concept maintains the use of a simple falling liquid curtain creating a cylindrical pocket around the RTL, but the configuration of this curtain has been modified substantially over the baseline Z-IFE curtain to account for the combination of larger power densities & damage limits inherent in the LLNL concept. To provide a total line thickness of 1 m, the annular flibe curtain, which has an areal density of 33%, extends from a radius of 1 m to 4 m from chamber center.

Figure 3.5.2 shows how the cross section of the curtain has been highly modified from the array of cylindrical jets depicted in FY04. This was carried out to enhance the venting of vapor from the central pocket region after a fusion pulses and reduce the form drag that results in threatening outward liquid motion. While the configuration now represents an educated guess at what preferable curtain geometry might look like, it is hoped that a combination of computer modeling and scaled experiments can verify this or even lead to a superior design.

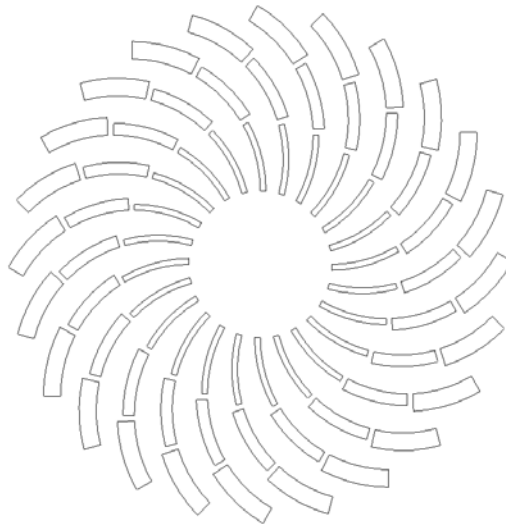


Fig. 3.5.2. A cross-section of the new liquid curtain array.

Figure 3.5.3 shows how instead of dumping into a static pool at the bottom of the chamber, the flibe curtain is now intercepted by a conical structure with fixed impulse turbine fins that direct the flow into a “quiescent” rotational motion in the toroidal accumulator that feeds recirculation pumps. This mitigates the danger of large splash-backs that could occur with highly disturbed slugs of flibe dropping into a deep static pool. In addition, this configuration recovers a significant portion of the kinetic energy of the falling flibe curtain as pressure to reduce pumping power requirements. These blades will have to be designed to withstand significant static and dynamic impact stresses from the falling liquid flibe after fusion events.

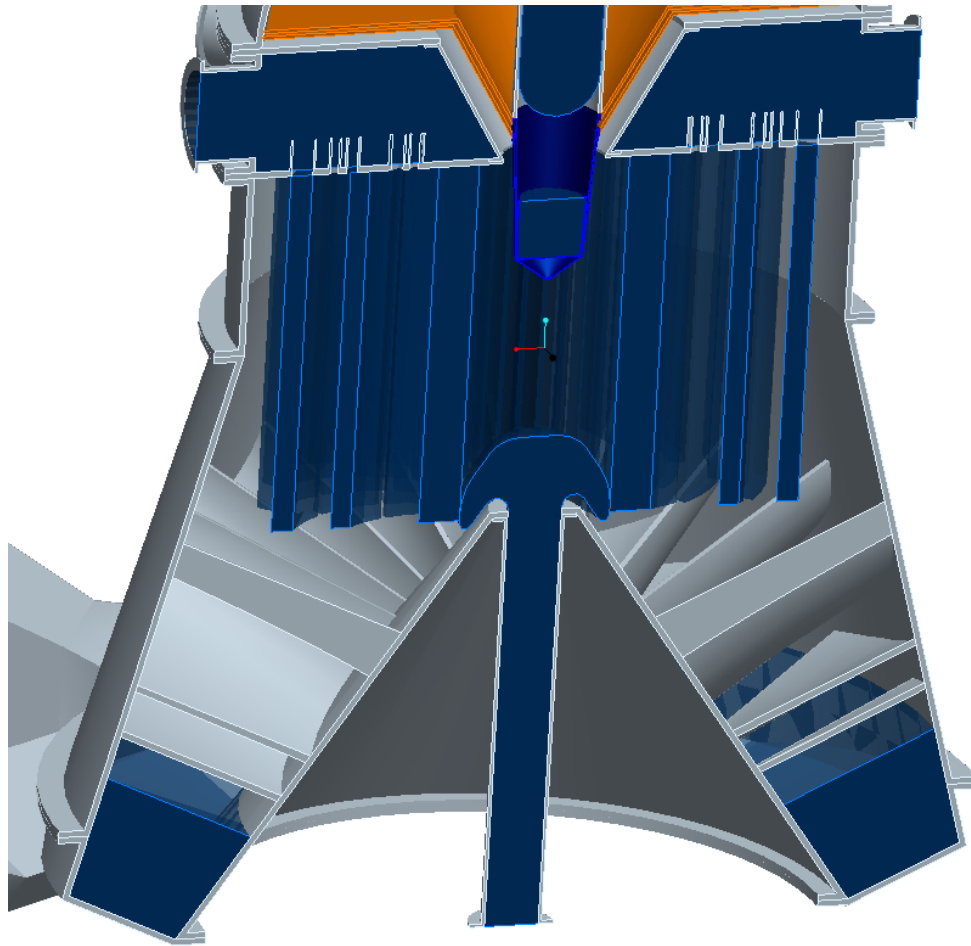


Fig. 3.5.3. The shielding curtain intercepts turbine blades to produce a “quiescent” rotational flow.

The solid structures in the central pocket below the target plane are protected from neutron damage by a stagnating liquid jet injected upward (also shown in Fig. 3.5.3 as proposed by the Russian Team). The flow from this jet joins the flibe curtain naturally at the bottom of the chamber before entering the recirculation system.

One of the more novel features of the shielding system is depicted in Fig. 3.5.4. It shows a bucket of flibe inserted with the RTL to shield chamber components above the shot plane that would otherwise be directly exposed to un-attenuated 14 MeV neutrons. At 10 m/s, the

downward momentum of this bucket of flibe overwhelms the upward impulse from the 4.6 GJ yield. If necessary, a falling slug of flibe is envisioned to counteract this motion.

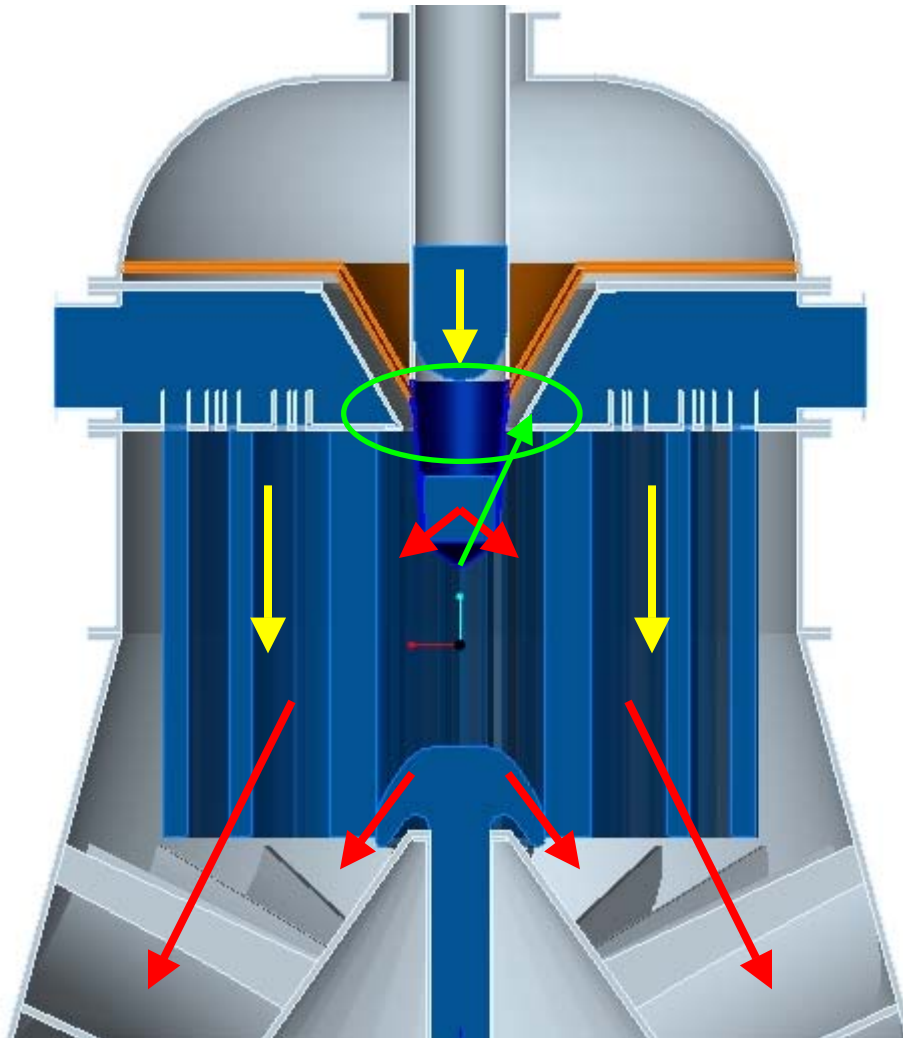


Fig. 3.5.4. An image of the flibe reservoir resident in the RTL at insertion time and the downward falling flibe slug. The yellow arrows indicate fluid motion prior to a fusion pulse and red arrows what is (roughly) expected to be the subsequent liquid motion. The green arrow and circle show the areas that will be protected from neutron damage by the RTL flibe reservoir.

3.5.5 Service and Maintenance

The overall shape and segmentation of the chamber concept was formulated with service and maintenance of internal chamber structures in mind. The top of the chamber is capped with a dome that can be removed when the MITL or MITL/RTL interface and locking mechanisms need to be replaced. The nozzle blocks and their associated flow conditioning can be accessed in the event of fowling or other blockage with the removal of the flibe inlet plenum just below the chamber dome. Once those components are removed, there is direct access to the impeller blades and flibe fountain injection hardware at the bottom of the chamber.

3.5.6 Concluding Remarks on Chamber Design

In this FY05 LLNL Z-IFE chamber design, we have attempted to incorporate several features that will enhance the performance of a Z-IFE power plant. The chief motivation has been to achieve greater power densities by making it possible to reduce the number of chambers needed for a net electric power output. The approaches that have been taken include selecting a high temperature, high thermal conductivity material for the FSW in C-C composite and going to higher rep-rates and larger target yields than the baseline design. To minimize the negative implications of these design choices, such as increased neutron fluxes and post fusion pulse liquid motion, the liquid curtain has been thickened to 1 m total line density and the FSW profile changed to allow for outward liquid motion while avoiding excessive liquid impulse on the wall. Other features have been added to reduce pumping power by converting the kinetic energy of the flibe flow into pressure energy. Upper chamber structures are protected from un-attenuated neutron radiation by a small pool (bucket) of flibe inserted with the cast flibe RTL.

3.6 Primary Loop Description

The carbon composite chamber, piping and heat exchanger system for Z-IFE as an alternative to the baseline steel version might have temperatures as given below appropriate for a Brayton power conversion cycle or hydrogen production. The temperatures might be high, but they are chosen as trial numbers because there does not seem to be a clear limit and larger temperature drops across heat exchangers make them smaller. The thermochemical cycle for hydrogen needs heat delivered at 850 °C. These numbers are appropriate for that application when one considers the temperature drop across the heat exchanger to the catalyst surface.

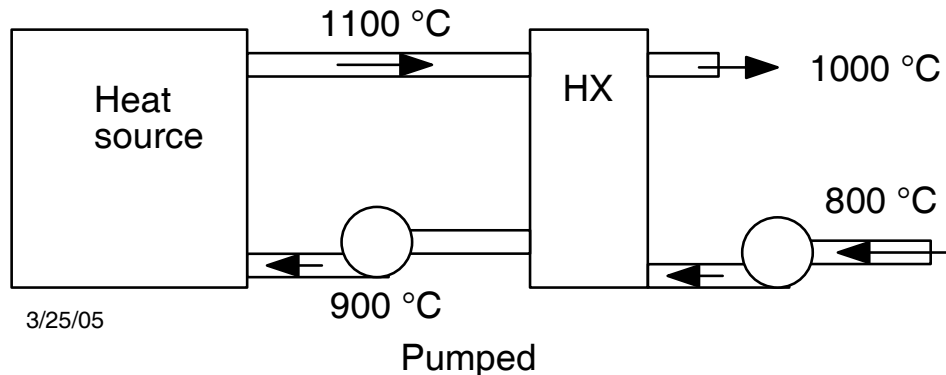


Fig. 3.6.1. Primary loop configuration and assumed temperatures.

The mass and volume flow rate to the heat exchangers to give 1000 MWe power is calculated below. The assumptions are shown in Fig. 3.6.1, and we assume the conversion efficiency at these high temperatures of 50% or even higher can be achieved.

$$P_{th} = \frac{P_e}{\eta_{th}} = \dot{m} \cdot c_p \cdot \Delta T$$

$$\dot{m} = \frac{P_e}{\eta_{th} \cdot (c_p \cdot \Delta T)} = \frac{10^9 J/s}{0.5 \cdot (2380 J \cdot kg^{-1} K^{-1} \cdot 200 K)} = 4200 kg/s$$

$$\dot{V} = \dot{m} / \rho = 4200 kg/s / 2000 kg/m^3 = 2.1 m^3/s$$

The flow rate of 2.1 m³/s to the heat exchangers is almost two orders of magnitude less than the flow rate to protect the walls. This means the jets will have a temperature just under 1100 °C and the 900 °C flow can be used for cooling components and for condensation sprays if desired.

3.7 Pumping Power

This section discusses pumping power for Z-IFE. The chamber configuration is given in Fig. 3.7.1. From the point of view of pumping power the important parameter here is fall height, h.

Rapid venting is important to minimizing acceleration of liquid. Slab jets are much better than round jets from this point of view. The vent path needs to be designed to minimize neutron streaming. Figure 3.7.2 illustrates examples of the idea. The important point in this figure is the area of jets to compute pumping power.

P = pumping power

h = height from pump inlet to nozzles + injection head, h'

h' = head above nozzles

v₀ = jet speed at injection nozzles assuming, height h'

v = jet speed at horizontal plane of the target g=acceleration of gravity = 10 m/s²

ρ = flibe density = 2000 kg/m³

\dot{V} = flow rate, m³/s

ε = jet packing fraction at the nozzles

L = areal liquid thickness

S = distance from nozzles to shot point=4 m

η_p = pumping efficiency = 0.8

η_{recovery} = head recovery efficiency = 0.5

R₁ and R₂ = inner and outer radius of jets array at the plane of the target.

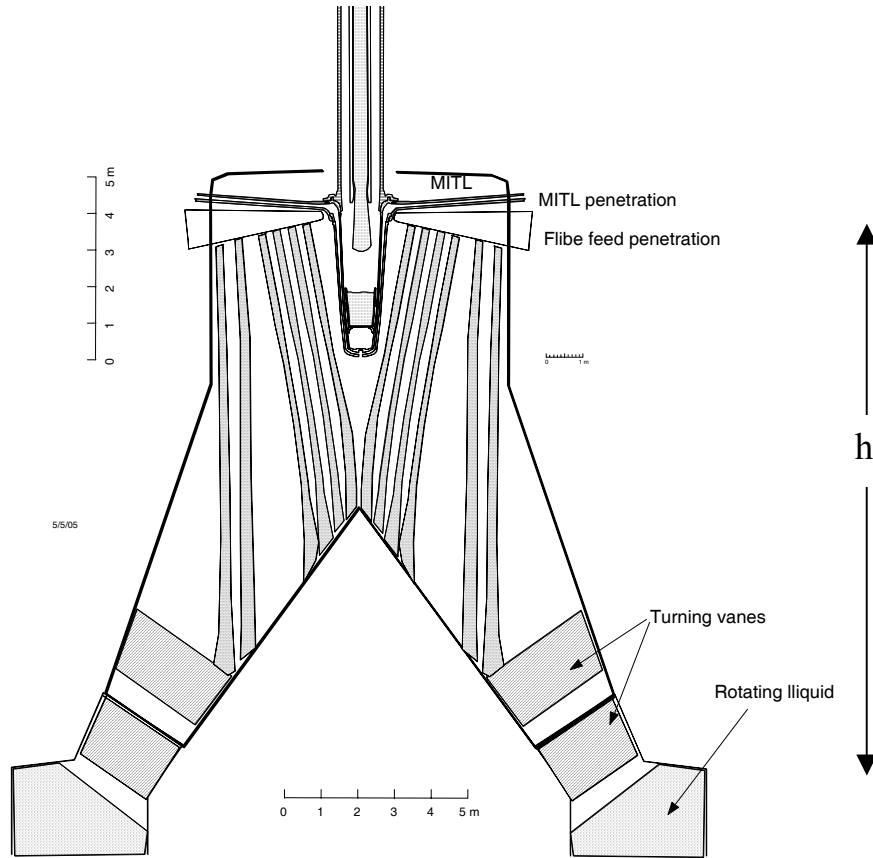


Fig. 3.7.1. Chamber with splash protection/no pool.

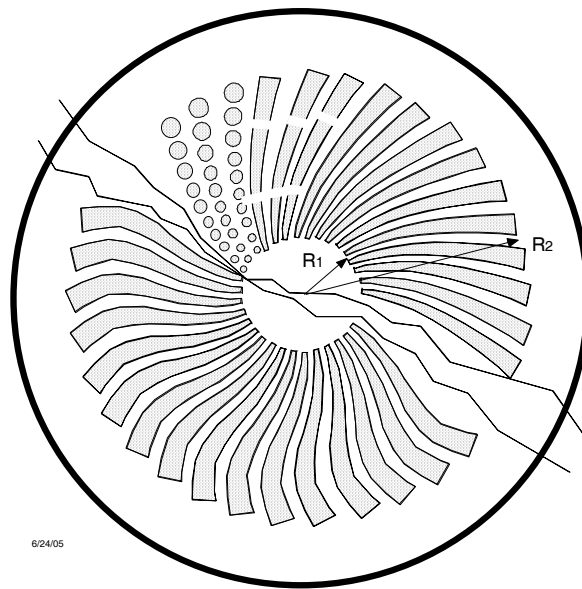


Fig. 3.7.2. Cross-section of jets at the plane of the target. Curved slab jets ease venting while keeping a high packing fraction. Two versions are shown with partial coverage and three rows with rounds jets are shown.

The power that has to be supplied to electric motors to pump the flibe to the reservoir assumed to be h' above the nozzles is:

$$P = \rho g h \dot{V} \left(\frac{1}{\eta_p} - \eta_{recovery} \right)$$

The areal thickness is:

$$L = (R_2 - R_1) \varepsilon_o \frac{v_o}{v}$$

$$\dot{V} = \pi(R_2^2 - R_1^2) \varepsilon v_o$$

$$v = \sqrt{v_o^2 + 2sg}$$

Example

$$h' = 2 \text{ m}$$

$$v_o = \sqrt{2sg} = \sqrt{2 \cdot 4 \cdot 10} = 6.32 \text{ m/s}$$

$$R_1 = 1 \text{ m}$$

$$R_2 = 4 \text{ m}$$

$$\varepsilon = 0.55$$

$$v = \sqrt{v_o^2 + 2sg} = \sqrt{6.32^2 + 2 \cdot 4 \cdot 10} = 10.9 \text{ m/s} \text{ velocity at midplane}$$

$$L = (R_2 - R_1) \varepsilon_o \frac{v_o}{v} = (4 - 1) \times 0.55 \frac{6.32}{10.95} = (4 - 1) \times 0.317 = 0.95 \text{ m}$$

This provides good neutron attenuation to protect the walls.

$$\dot{V} = \pi(R_2^2 - R_1^2) \varepsilon v_o = \pi(4^2 - 1^2) 0.55 \cdot 6.32 = 25.9 \text{ m}^2 \times 6.32 \text{ m/s} = 164 \text{ m}^3 / \text{s}$$

Suppose the liquid height, h is 8 m including the head above the nozzle plate. This is shorter than that shown in the figure above and is a guess at where the shorter RTL and reduced size chamber will end up. Then the pumping power is:

$$P = \rho g h \dot{V} \left(\frac{1}{\eta_p} - \eta_{recovery} \right) = 2000 \cdot 10 \cdot 8 \cdot 164 \left(\frac{1}{0.8} - 0.5 \right) = 26.2 \text{ MW} (0.75) = 20 \text{ MW}$$

The pumping power supplied by electric motors for the jets is 33 MW without head recovery and 20 MW with head recovery.

Suppose we decided to turn the liquid flow off to save pumping power during part of the impulsive time. In this case the flow could be turned off at the time the liquid arrives at the apex

of the inverted cone diverter. From Fig. 3.7.1 we estimate this fall distance to be about 6 m. The time fall t is:

$$t = \frac{-v_o + \sqrt{v_o^2 + 2hg}}{g} = \frac{-6.32 + \sqrt{6.32^2 + 2 \cdot 6 \cdot 10}}{10} = 0.63s$$

For an interpulse time of 1.6 s, the average flow rate, therefore average pumping power would be $0.63/1.6 = 0.39$. The 20 MW above would come down to 7.8 MW.

If we substitute LiPb at $\rho = 9000 \text{ kg/m}^3$ for flibe with the same thickness of jet array, the pumping power of 20 MW above for flibe would increase by the ratio of 9000/2000 to 90 MW. However, LiPb is about half as effective at protection of the wall material from neutron damage at the same 1 m thickness. If the flow rate were stopped after 0.6 s in the above example of a 1.6 s interpulse time, the 90 MW would drop to 34 MW, which is still a large pumping power.

In conclusion, the jets should protect the walls (~1 m flibe thickness) and yet clear the chamber rapidly allowing a time between pulses of less than 2 second. Getting the target and recyclable transmission lines in place will be limiting rather than chamber clearing. With the pool chamber, splash back will likely be a limit in pulse rate. The idea is to contain the fusion energy release with the aid of liquid jets without the liquid striking the sidewalls.

3.8 Chamber with Minimal Gas Pressure as Alternative to ~20 Torr of Inert Gas

We recommend operating with a background pressure of non-condensable gases of less than 10^{-5} Torr as an alternative to the baseline design of 20 Torr of inert gas. Low pressure allows cryogenic pumping of tritium, ease of maintaining the $<10^{-5}$ Torr in between the inner and outer cones of the RTL required for good power transmission. High pressure (20 Torr) poses a difficult tritium removal problem and poses difficult design problems for the RTL. The vapor pressure and evaporation (condensation) rates as given in Appendix A.3.

3.9 Tritium Recovery System and Tritium Inventory

The idea developed in HYLIFE-II and recommended for Z-IFE for tritium handling is to process the flibe stream that is going to the heat exchangers to such a low level of tritium that the loss to the water side of the heat exchanger meets the goal, 40 Ci/d at that time. For safety reasons and to limit the amount of leaking water into the flibe to a low level double-walled tubes were selected to keep the chance of a single crack from failing any one tube. The inner space was not purged.

Studies [5] suggested two vacuum disengagers in series could reduce the tritium concentration sufficiently. The vacuum disengager is an alternative design to the Z-IFE based case of 20 Torr of background gas with its high amount of dissolved gas. This safety of the system should be very similar to that of HYLIFE-II [6,7].

For the carbon composite alternative material the new issue of tritium inventory comes up. Appendix A.2 discusses the tritium inventory in the carbon wall under various assumptions. With a silicon carbide layer 10 mm into the carbon composite wall that prevents exposure of the bulk of the material to tritium buildup, we calculate a 20 mg tritium inventory due to solubility and a 32 g inventory due to the trapping mechanism after modest irradiation of only 0.1 dpa. If the SiC layer were not used this number would increase by a factor of about 5 for a 50 mm thick wall. One reason the inventory is so low is the almost a factor of 100 isotopic dilution of tritium by hydrogen due to the liquid hydrogen reservoir included in each target. This will add greatly to the pumping and isotopic separation system. If the liquid hydrogen reservoir is eliminated, the tritium inventory goes up to 94 g for the 1 mm layer case and 940 g for the 10 mm case.

Based on a tritium inventory in carbon of 32 g and assuming that all the tritium was to be released in an accident (case of complete oxidation of C/C structures), we have estimated an off-site dose ~ 1.5 rem, assuming conservative weather conditions. This dose would be 10 \times lower if release occurs through 100 m elevated stack.

3.10 Neutronics – Direct Conversion from CAD to Monte Carlo

Designers spend a great deal of time and effort on the generation of computer assisted design (CAD) models. Typically, these designers develop a model and then hand off a stack of drawings to a neutronics analyst, who turns that stack of drawings into a simplified model that attempts to portray the important features without going into unnecessary detail. The methods used to generate the neutronics model are, by comparison to what is available to the CAD community, incredibly primitive. Simple combinatorial geometry via textual input is the norm. The effort is not only duplicative, but it is tedious and prone to error.

A fundamental step-change in the way neutronics analyses are performed would occur if one were able to directly generate neutronics models, in an automated fashion, from existing CAD models. This would not only reduce duplication of effort, but it would improve accuracy. More important, direct conversion from CAD to Monte Carlo would change the way in which neutronics analyses are done. Neutronics considerations would be better positioned to weigh in during the design phase of a project rather than simply analyzing the final or near-final design.

Raytheon is coming close to achieving this vision. They have developed the TOPACT code, which converts CAD STEP files (that can be created by nearly any major CAD program) TART and MCNP input files. Development of TOPACT continues, so the code is not yet a pushbutton system. Nevertheless, we felt that a modest contract with Raytheon was appropriate at this time. We have asked Raytheon use TOPACT to complete several test problems of interest to our various programs.

Originally, the contract included two test problems: an ITER diagnostic and a component of the NIF target positioner, called the clamshell. With these first two problems we learned that many CAD models, especially those for systems still under development, are not "clean" in that they are not interference free. Each model had hundreds of interferences ranging from light rays going through optics to fasteners going through parts that they were to fasten together. A significant amount of effort was required to clean up the NIF clamshell model. Work continues in our attempts to produce a usable model for the ITER MSE diagnostic.

Once the CAD model was updated, the conversion process in TOPACT went fairly smoothly. Figure 3.10.1 shows plots of the NIF clamshell model. The plot on the left was generated in Pro|Engineer, while the plot on the right was generated using TART's geometry code, TARTCHEK, once Raytheon provided the TOPACT-generated input file. The TART model has 1059 surfaces and 2308 zones. Despite all of this detail, the radiation transport runs very quickly. This is due to the fact that the various zones are relatively simple geometrically.

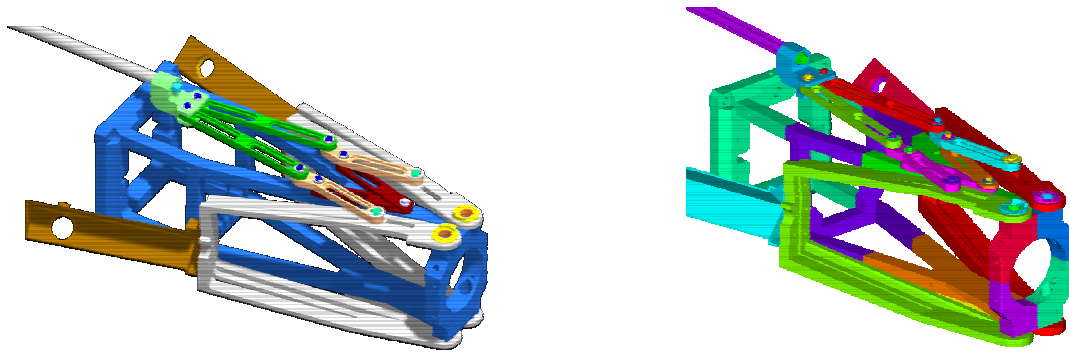


Fig. 3.10.1 TOPACT was used with Pro|Engineer CAD files of the NIF clamshell (left) to generate a TART input file for use in radiation transport calculations (shown on the right).

Given the difficulties experienced with pre-existing CAD models, we felt that a fairer test of TOPACT's capabilities might be achieved using our newly-created Z-IFE chamber model. We ensured that the model was interference-free and that Raytheon's recommended procedures were followed. The complexity of our Z-IFE model still caused some difficulties for TOPACT. In the end, however, a usable neutronics model was generated. The Pro|Engineer and TARTCHEK plots are shown in Fig. 3.10.2.

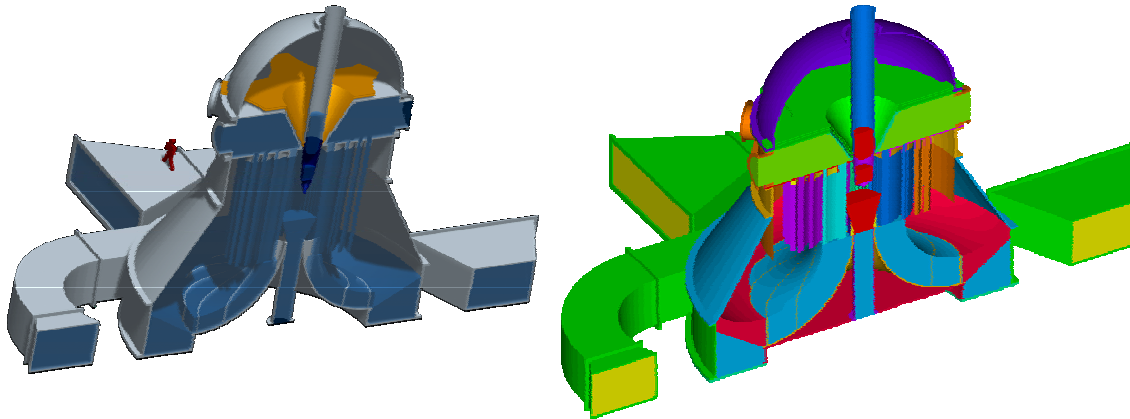


Fig. 3.10.2. TOPACT was used with Pro|Engineer CAD files of LLNL's Z-IFE chamber design (shown on the left) to generate TART files of the same (shown on the right).

The TART input file for LLNL's Z-IFE chamber design uses over 1200 surfaces and about 3600 zones. At the time of this report, some interferences remain to be resolved, and the Z-IFE calculation was not yet complete.

3.11 Choice of High-Z Material - Advantages and Disadvantages of Hg, Pb and W

3.11.1 Introduction

IFE requires high-Z materials for the hohlraum and in the case of the Z IFE for the Z-pinch wires. Gold and tungsten are used in experiments for practical reasons, however, for a power plant ease of recovery and recycle and cost become important issues to deal with. A problem with gold is cost and difficulty of recovery. Lead should be low cost but have the same recovery problem as gold. Both gold and lead can attack construction materials at high temperatures (>500 °C). Use of tungsten involves complex chemical recovery methods whose costs are uncertain. Also clogging of narrow channels might become an issue. Mercury by contrast should be both low cost and easy to recovery. Its chemical hazard will always be an issue to deal with as will its necessity to handle at low temperatures. In what follows we discuss some properties of mercury of interest to possible Z-IFE application to coat surfaces of the hohlraum and to make wires by extrusion both at low temperature (< -40 °C).

Both Hg and Pb have been suggested for use in Z-IFE targets. HIF target studies showed that chemical toxicity is more critical than radiotoxicity for both Hg, Pb [8]. Although both materials have similar air-concentration limits for public protection, the high volatility of mercury is a concern in case of accidental releases. Flibe processing studies suggest Hg inventory is 1000x smaller than Pb (7 kg vs 7000 kg). Thus, in spite of its volatility, mercury would appear as a safer option than lead from the point of view of accidental coolant spills.

Regarding the target fabrication facility, in the case of Z-IFE we estimate a target supply rate ~6x lower than HIF case, however, the mass per target is ~12x larger. This gives us 2x higher inventories for Z-IFE. Therefore, segregation of inventories and optimization of target fabrication plant layout will be critical to minimize accidental releases.

3.11.2 Tensile Strength of Mercury Versus Temperature

The tensile strength of mercury is given in Fig. 3.11.1 for various temperatures [9]. The data was taken for either four or five samples at the three temperatures shown. As the strain was increased in the 1.6-mm-diameter wire sample, the stress increased to a maximum and then decreases. The peak can be inferred as the breaking strength or tensile stress. Various samples break at different stresses. This is due according to the authors to the distortion of the grains and phase changes during strain. From a practical point of view we can assume wires are useable if we stay below the shaded curve and wires can be made by extrusion at pressures above the shaded curve.

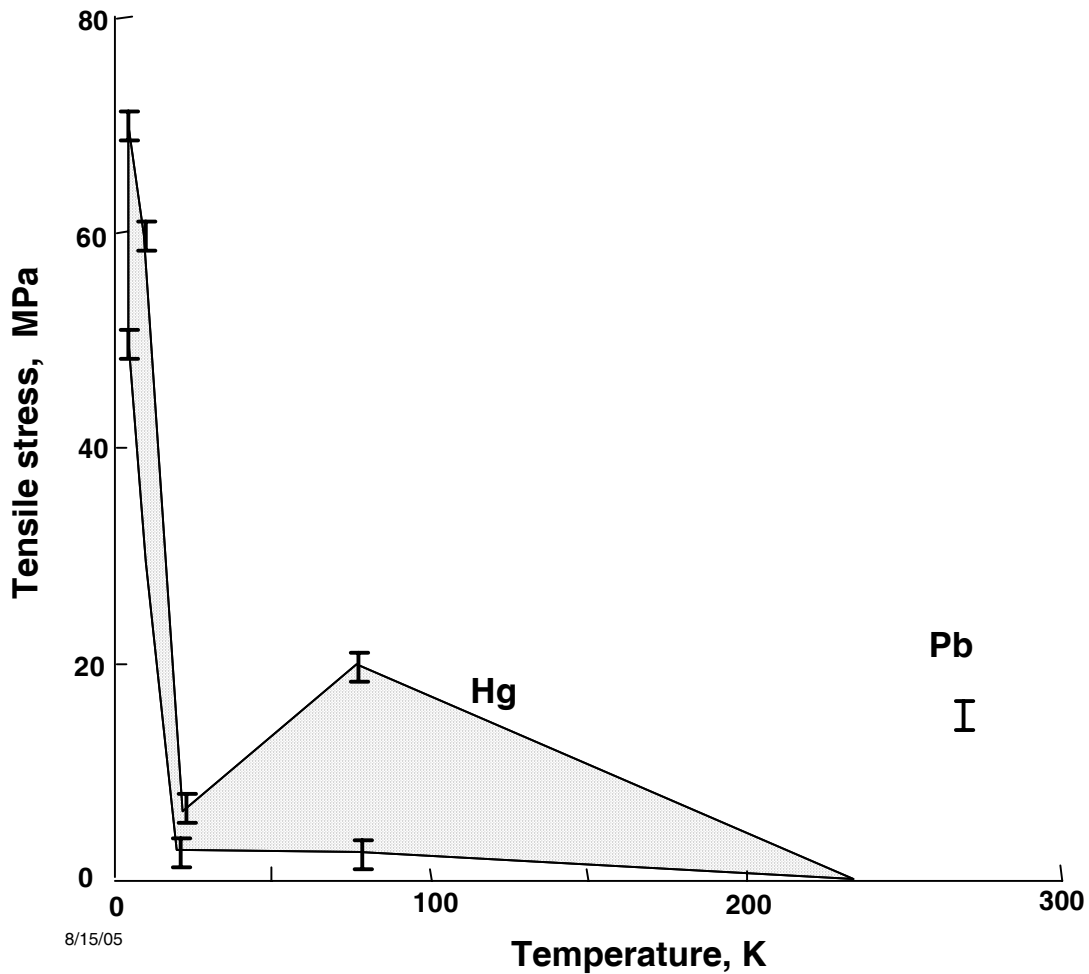


Fig. 3.11.1. Tensile strength for mercury wires

For comparison we show the tensile strength at room temperature for lead, which has about the same strength as mercury at 77 K. The strength of mercury goes to zero at its melting point of 234 K just as the strength of lead goes to zero at its melting point of about 600 K.

3.11.4 Evaporation Rates of Mercury

Mercury has a high vapor pressure and little chemical interaction with flibe, so that recovery should be straightforward by distillation followed by condensation. This is especially attractive if the same method is employed to remove and recover tritium by the same method in a vacuum disengager. Therefore we develop some useful numbers for the analysis of mercury recovery.

The vapor pressure for mercury fitted to data in reference [10] and evaporation rates are calculated from the following equations and plotted in Fig. 3.11.2:

$$P = e^{(A-B/T)} = \text{pressure in Pa.}$$

$n = \frac{p}{kT}$ = equilibrium vapor density in atoms/m³.

$$J = \frac{n\bar{v}}{4} = \frac{p}{(2\pi m kT)^{0.5}} = CT^{-0.5} e^{(A-B/T)} = \text{evaporation rate in atoms/m}^2\text{s}.$$

$$mJ = \frac{n m \bar{v}}{4} = \frac{(m)^{0.5} p}{(2\pi kT)^{0.5}} = DT^{-0.5} e^{(A-B/T)} = \text{evaporation rate in kg/m}^2\text{s}.$$

Here, A=23.25, B=7,400 and C=1.86×10²³, D=0.0619 and k=1.38×10²³ J/K. The density and evaporation rates are shown in Fig. 3.11.3 to 3.11.5.

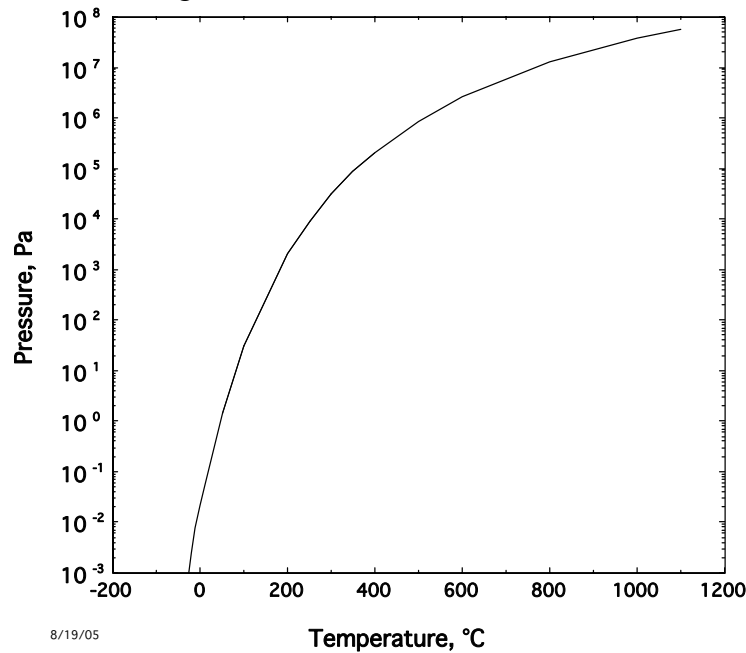


Fig. 3.11.2. Vapor pressure of Hg.

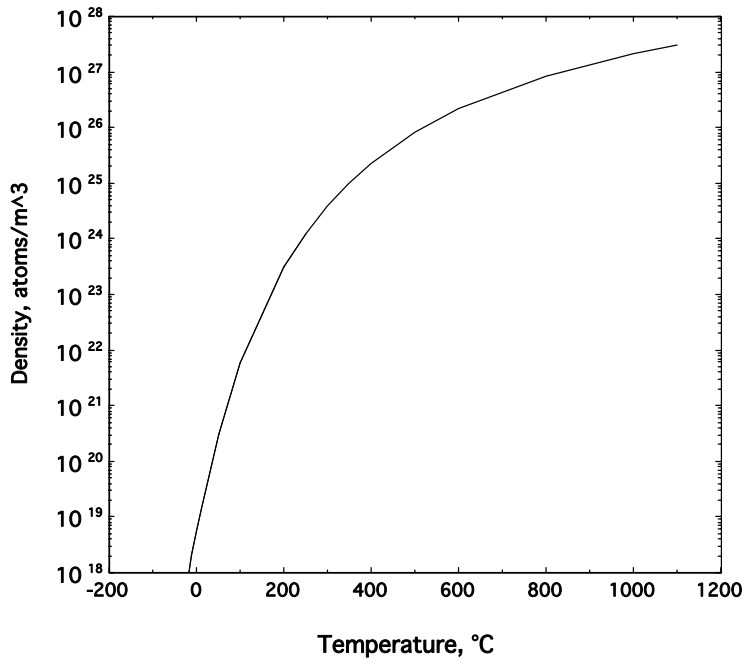
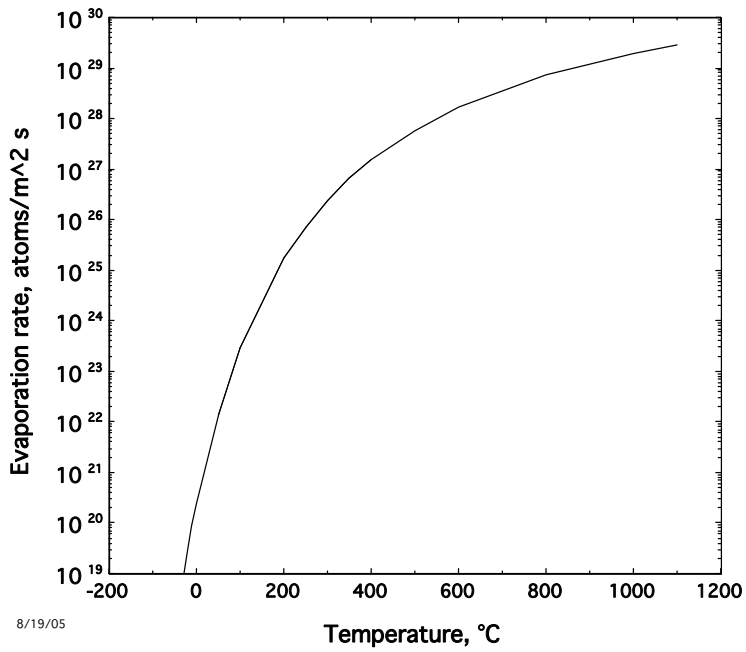


Fig. 3.11.3. Equilibrium vapor density.



8/19/05

Fig. 3.11.4. Atomic evaporation rate.

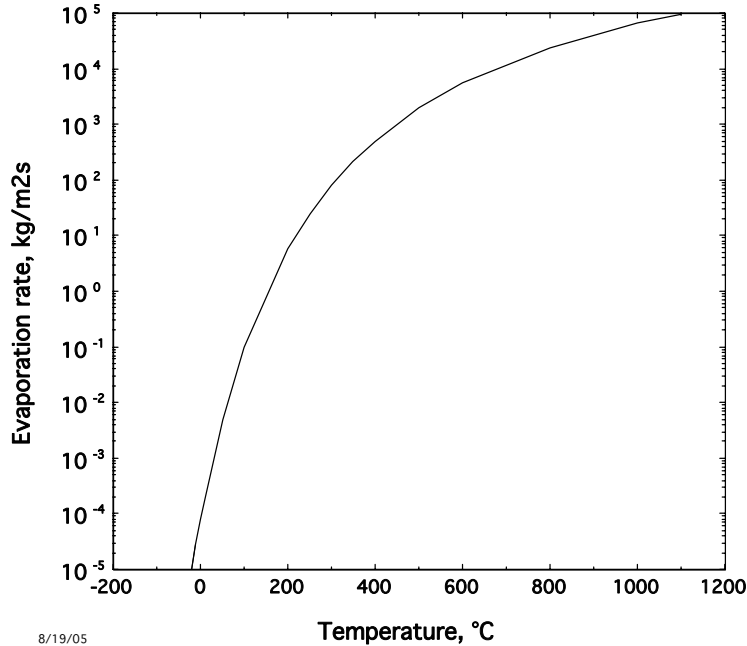


Fig. 3.11.5. Mass evaporation rate.

For IFE, the temperature of interest for a steel chamber is about 650 °C and for a carbon composite chamber more like 1100 °C. If the Hg is mixed with the flibe at 1 ppm then the equilibrium vapor pressure is a few Pa at 650 °C and under 100 Pa at 1100 °C as shown in Fig. 3.11.2. (For reference, the pressure in Pa is 133.3 times the pressure in Torr.) Similarly the evaporation rate might be about ten grams per second per square meter at 650 °C and 100 g at 1100 °C. A few square meters of pumping area should be sufficient to remove the mercury at the 1 g per shot rate it is generated. If the concentration of Hg in flibe is 1 wppm, the Hg vapor density is $\sim 3 \times 10^{20} / \text{m}^3$ at 650°C. The question is if this is an issue or not. Detailed analyses of the removal of mercury by volatility and condensation might result in far lower inventories than that just assumed and such analyses should be carried out.

3.12 Flibe Cleanup and High-Z Material Recovery for Recycle

The molten salt, flibe, in the Z-IFE will have to be processed to remove target material and contaminants from leaks and corrosion products. This subject has been discussed in a previous report on HYLIFE-II processing from which much of the present discussion is based [10]. The target will contain high-Z material, beryllium, oxygen, carbon, and hydrogen isotopes. Oxygen from air and water leaks and outgassing from materials will need to be continually removed as well. The processing plant needs to be considered when making decisions on material choices in the plant. For example, some tritium recovery methods oxidize the T to T₂O. This would put a burden on the processing plant to remove the oxygen. The choice of high-Z material, W, Pb or Hg will have a strong impact on the processing plant. Chemical processing and related topics are discussed in Sections 3.9, 3.11 and Appendix 6.4.

3.13 Thermal Stress in Chamber Walls

In HYLIFE-II the thermal stress in 304 SS wall of 5 cm thickness behind 1 m of flibe required one layer of internal cooling. Ferritic steel has higher thermal conductivity and the wall is further away so Z-IFE will be better off. However with the baseline design of only 0.5 m of flibe, the heating in the steel will be high (if we try to get 1000 MWe out of one chamber) requiring the wall to be divided into many layers for internal cooling inside the wall. This design tradeoff of flibe thickness and thermal stress in the steel wall is an important topic if we want to use one chamber and use minimum flibe in the jets.

3.14 Output from Z-IFE Targets

We have performed a series of 1-D calculations to explore output from Z-IFE targets and to explore methods for controlling output from Z-IFE targets. Having some control over the output, e.g., trading off radiation energy versus kinetic energy of the debris and/or control over the directionality of the output, can be a valuable tool for designing chambers that are able to withstand the large blasts at reasonably high repetition rate.

As a first cut, we have done 1-D output calculations for a capsule that produces 2.9 GJ of yield. The 1-d capsule is a slightly modified version of the one proposed by R. Olson [12]. It uses a beryllium ablator doped with 0.4% copper. The capsule dimensions are shown in Fig. 3.14.1. The capsule is driven by the temperature shown in Fig. 3.14.2 – with a peak drive of 260 eV. The hohlraum is assumed to have a case-to-capsule ratio of 3 (i.e., the hohlraum radius is three times the capsule radius).

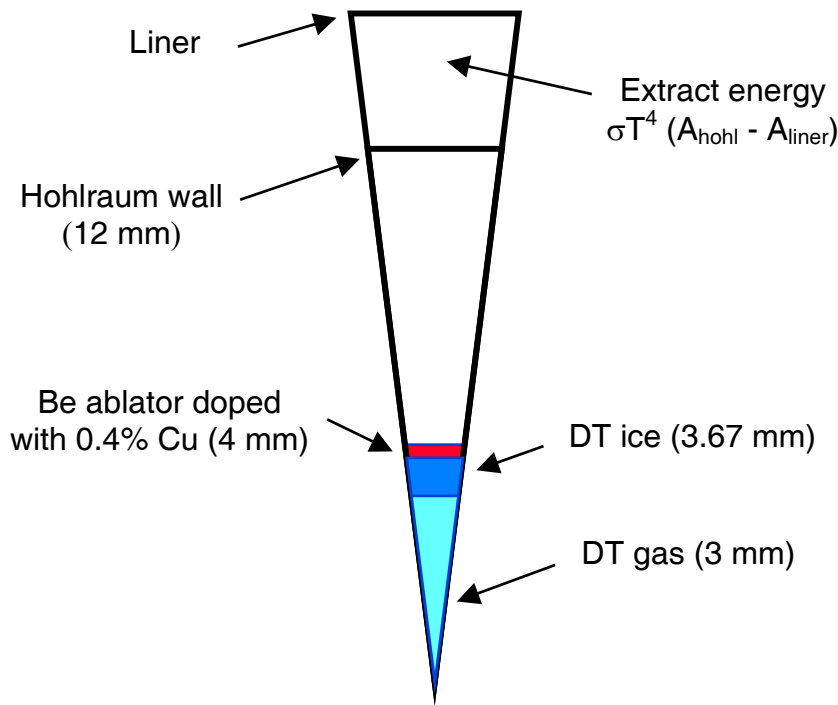


Fig. 3.14.1. Schematic of 1D target configuration.

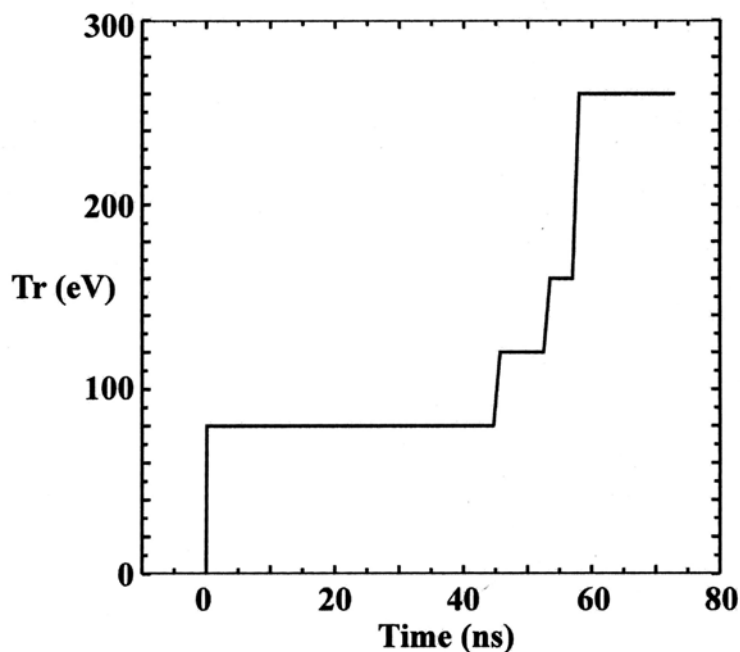


Fig. 3.14.2. Drive temperature profile for Z-IFE target.

Our ‘nominal’ target has a hohlraum wall thickness of 20 microns. This is enough material to contain the radiation drive during the time of the implosion. In the case of the double-ended Z-pinch hohlraum, we are free to increase the thickness of the hohlraum without affecting the target physics. In the dynamic hohlraum, the wire arrays form the hohlraum so increasing the thickness would change the target physics. It may be possible to put the dynamic hohlraum target into an additional enclosure to allow flexibility in the hohlraum wall thickness, however.

Table 3.14.1 shows how the output energy is partitioned between neutrons, radiation, kinetic energy of the debris, and thermal energy of the debris for three hohlraum wall thicknesses. The third case, 200 micron thick wall, shows how we can change the balance between debris and radiation.

Table 3.14.1 Target Output for Various Hohlraum Wall Thicknesses

Hohlraum wall thickness	20 micron	50 micron	200 micron
Neutron energy	69%	68%	64%
Radiation energy	27%	28%	16%
Debris kinetic energy	4%	4%	16%
Debris thermal energy	<1%	<1%	3%

Chamber designers might also like to be able to direct the output – for example, they may want to direct radiation energy away from the top of the chamber where the transmission lines come in. Based on an idea proposed by Per Peterson (UC Berkeley), we tried to model a target

in which some fraction of the hohlraum is surrounded by a thick shield. The idea was to block radiation in the direction of the shield.

Since these initial calculations were 1-D, we make an approximation to the 2-D geometry by surrounding the hohlraum with a shield, then extracting energy from the region between the hohlraum wall and the shield to model the radiation that will escape from the region of the hohlraum that is not covered by the shield. If we do not extract energy in this way, then, in 1-D, the shield will have the same effect as the thicker hohlraum shown above.

Table 3.14.2 shows the results for a 20 micron thick hohlraum with a 100 micron thick shield placed 1 mm outside the hohlraum wall for shields that cover 0% (no shield), 25%, and 50% of the area around the hohlraum. From the table, we see that even a shield that covers 50% of the area still allows radiation to flow freely through the remaining 50% of the area. The shield seems quite effective at blocking radiation since less than 1% of the energy get through the shield.

Table 3.14.2 Radiation Flow for Various Shield Fractions

	0% shield	25% shield	50% shield
Neutron energy	69%	65%	65%
Radiation energy through shield		< 1%	< 1%
Rad. energy thru unshielded area	27%	33%	32%
Debris kinetic energy	4%	3%	3%

Although these 1-D calculations are an approximation (and, hence, certainly not good to the 1% level), we note that the shield seems to reduce the kinetic energy of the debris slightly. This seems to occur because the expanding hohlraum collides with the shield and some of the hohlraum kinetic energy is converted to radiation. Additional analyses are needed to determine the effect on upward impulse, which is the key concern.

This 1-D study points the way for future work on output for Z-IFE targets. It shows that we can change the balance between energy that comes out in radiation versus energy that comes out in debris. Being able to change the form of the output may be useful for chamber designers. In addition, the use of a shield to prevent radiation from being directed towards the transmission lines seems promising. These results should be folded in with the chamber design so that we can determine which target configurations we want to study with more detailed 2-D calculations.

References for Section 3

- [1] S.A. Slutz, C.L. Olson, P. Peterson, “Low mass recyclable transmission lines for Z-pinch driven inertial fusion,” *Physics of Plasmas*, **10** (2003) 429-4337.
- [2] W.R. Meier, “Osiris and SOMBREREO inertial fusion power plant design—summary, conclusions and recommendations,” *Fusion Eng. Des.*, **25** (1994) 145-157.
- [3] S. Reyes, J.F. Latkowski, J. Gomez Del Rio, J. Sanz, “Accident Doses Analysis of the Sombrero Inertial Fusion Energy Power Plant Design,” *Fusion Technology*, **39**, (2,2) 941-945 (2001).
- [4] T.D. Marshall, et al., “Oxygen reactivity of a carbon fiber composite,” *Fusion Engineering and Design*, **69**, 663-667 (2003).

- [5] T.J. Dolan, G.R. Longhurst, E. Garcia-Otero, “A vacuum disengager for tritium removal from HYLIFE-II reactor flibe,” *Fusion Technology*, **21** (1992) 1949-1954.
- [6] S. Reyes, J. F. Latkowski, J. Gomez Del Rio, J. Sanz, “Accident Consequences Analysis of the HYLIFE-II Inertial Fusion Energy Power Plant Design”, *Nuclear Instruments & Methods In Physics Research Section A*, **464** (N1-3): 416-421, (2001).
- [7] S. Reyes, J.F. Latkowski, J. Gomez Del Rio, J. Sanz, “Progress in Accident Analysis of the HYLIFE-II Inertial Fusion Energy Power Plant Design,” *Fusion Technology*, **39**, (2,2) 946-950 (2001).
- [8] S. Reyes, J.F. Latkowski, L.C. Cadwallader, R.W. Moir, J. Gómez Del Río, J. Sanz, “Safety Issues of Hg and Pb as IFE Target Materials: Radiological Versus Chemical Toxicity,” *Fusion Science and Technology*, **44**, 400-404 (2003).
- [9] S. Purushothaman and T. Caulfield, “Cryogenic temperature mechanical behavior of solid mercury,” *J. Appl. Phys.* **55** (1984) 3863-3865.
- [10] D. E. Gray, Coordinating Editor, *American Institute of Physics Handbook*, Second Edition McGraw-Hill Book Company, New York (1963) p4-282.
- [11] R.W. Moir, “Flibe coolant cleanup and processing in the HYLIFE-II inertial fusion energy power plant,” LLNL Report UCRL-ID-143228 (2001).
www.osti.gov/servlets/purl/15006180-1kse4O/native/
- [12] R. E. Olson, *Fusion Science and Technology*, **47**, 1147 (2005).

4. Findings and Recommendations

4.1 Summary of Findings

Based on our work in FY05, we find that there are many design options for Z-IFE that, if proven feasible, could lead to a more attractive system than the previously proposed baseline design. LLNL has proposed and analyzed:

- Use of a frangible flibe RTL instead of steel
- Dynamic insertion of the RTL where electric connections are made while the RTF is dropping into the chamber
- An alternative chamber configuration that eliminates the pool at the bottom
- Use of C/C composites for the chamber material instead of steel
- Operating the chamber a low background pressure (10^{-5} Torr instead of 20 Torr)
- Operating at the maximum possible yield and pulse rate to minimize the number of chambers needed to supply the total plant electrical output.

Eliminating the pool is important if we want to get a high pulse rate of up to 0.6 Hz. A pool may be acceptable at 0.1 Hz rate, but one would have to worry about how to dissipate energy to avoid splashing even after 10 seconds. Based on economic studies, we believe a high pulse rate is necessary so we recommend the loop chamber concept be adopted. The feasibility of carbon composites for the chamber rests on research to be successfully carried out in the next decade or so. Today we do not know how to make the carbon composites tritium tight but we have ideas such as use of SiC barriers and glassy carbon coatings. We don't know how to join the chamber to pipes with flanges that are sealed. We don't know how to repair chamber components or pipes. Flat plate heat exchangers made of carbon composites are not available today but we have untested designs. Also the related development of carbon composite for membranes for high temperature electrolysis and fuel cells and other applications will contribute to the feasibility for Z-IFE use. We recommend the Z-IFE team keep the carbon composite as a higher performing alternative option that includes hydrogen production and Brayton cycle electricity production. The flibe RTL has many advantages compared to steel, but also many issues to be addressed.

4.2 Summary of Recommendations

Although we have made good progress on this alternative design concept, in most cases more detail design and analyses, significant development, experiments on specific phenomenon, and proof of concept experiments will be required. Specifically we recommend the following:

Flibe RTL

Significant work is needed to address key issues associated with the use of flibe for the RTL, but the benefits are so compelling that development should be given high priority within the Z-IFE program. Proposed work includes:

- Experiments to investigate methods of producing frangible flibe RTLs, including casting in carbon composite molds as suggested here.
- Experiments to simulate the mechanical loads and response of the RTL (e.g., maintaining the gap tolerance between inner and outer cones during dynamic insertion). Include the investigation of the ability to make adequate electric contact during dynamic insertion.

- Further analyses and experiments on conductivity of flibe RTL and ability to handle the required currents. Include evaluation of need for a conducting coating.
- Integrated optimization of the RTL design considering mechanical and nuclear as well as electrical performance to achieve long component life, low cost of the pulse power system and good overall economics.

Carbon Composite Structure

One of the key concerns with respect to the use of carbon composites is limiting the amount of tritium that is trapped and the resultant tritium inventory. Recommendations include:

- Material development to demonstrate the ability to embed a thin SiC layer to form a tritium barrier.
- Tests to evaluate the effectiveness of the proposed SiC layer as a permeation barrier, including possible degradation due to cracking resulting from pulsed mechanical loading.

Although we have made good progress on this alternative design concept, in most cases, more detail design and analyses, significant development, experiments on specific phenomenon, and proof of concept experiments will be required. Specifically we recommend the following:

Appendix A.1

Thermal Stress During Insertion and Casting of RTL

Casting and Insertion of RTL

The RTL could be made of frozen flibe. The conical shaped RTL inner cone and outer cone might be made by pouring molten salt at about 500 °C into a carbon composite mold whose temperature is about 20 °C. When the RTL is inserted into the chamber it will see a flibe vapor at about 650 °C for the SNL baseline design or up to 1100 °C for the carbon composite chamber design. One concern is surviving the thermal shock for both these cases.

Temperature Response During Casting

The temperature in the wall as a function of distance x from the center of the wall is given below [1]:

$$\frac{T_i - T}{T_i - T_f} = \frac{500^\circ C - T}{500 - 480^\circ C} = 1 - \frac{4}{\pi} \sum_{n=0}^{\infty} \frac{(-1)^n}{(2n+1)} \cos\left(\frac{(2n+1)\pi x}{2l}\right) e^{-\frac{(2n+1)^2 \pi^2 \alpha t}{4l^2}}$$

$$\alpha = \frac{k}{\rho C} = \frac{1 \text{ W/mK}}{2000 \text{ kg/m}^3 \cdot 2380 \text{ J/kgK}} = 2.1 \times 10^{-7} \text{ m}^2 \text{ s}^{-1}$$

For a 3 mm thick wall cooled from both sides, $l = 1.5$ mm.

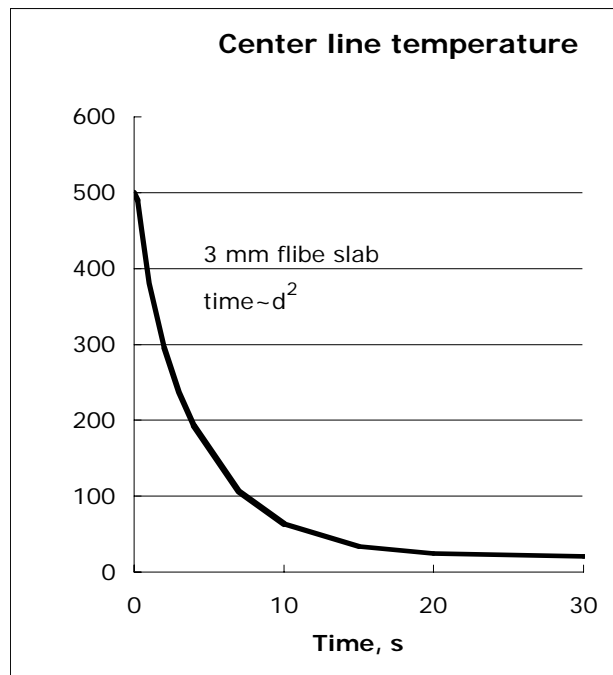


Fig. A.1.1. Center-line temperature in the wall of the casting versus time after the pour.

Pure conduction is assumed with no thermal resistance at the interface between the carbon composite and the cooling molten salt. We could assume a gas gap and see if this causes significant thermal resistance. One issue is the contraction on cooling of the frozen salt will be more than that of the mold.

We can calculate thermal stress from the above space and time dependent formula for temperature (see below).

Molds for Flibe Castings

The mold for the flibe castings could be made of carbon composites. The thermal conductivity of carbon is about 100 times that of flibe. The flibe as a liquid would be injected into the mold at about 500 °C and would cool in about 10 seconds (as can be seen from the figure above) if it were 3 mm thick. A wall thickness of 3 mm was rather arbitrarily chosen but might be much thinner. The cooling time is proportional to the thickness squared. The interior shapes such as ribbing need to be worked out as well as mold design to aid quick disengagement. If the thermal stress on cooling is excessive causing cracking, the inevitable gas gap with its thermal resistance could be included in the analysis. Also the temperature of the mold could be raised from the assumed room temperature.

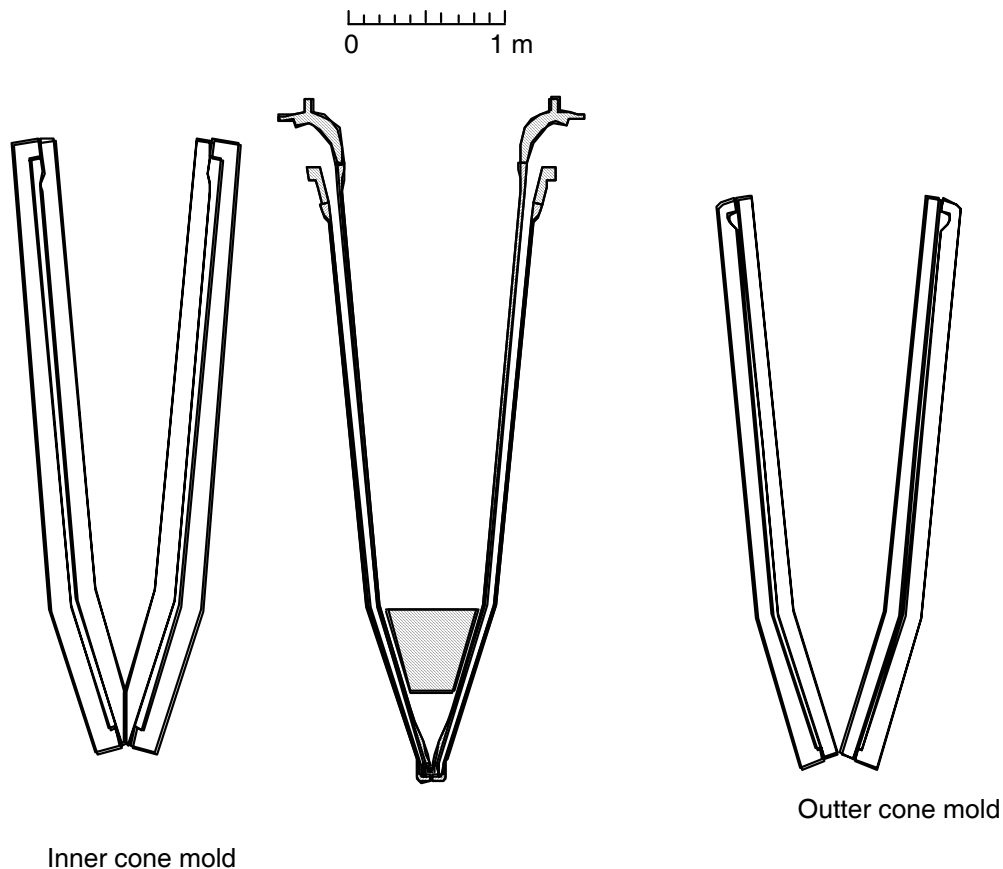


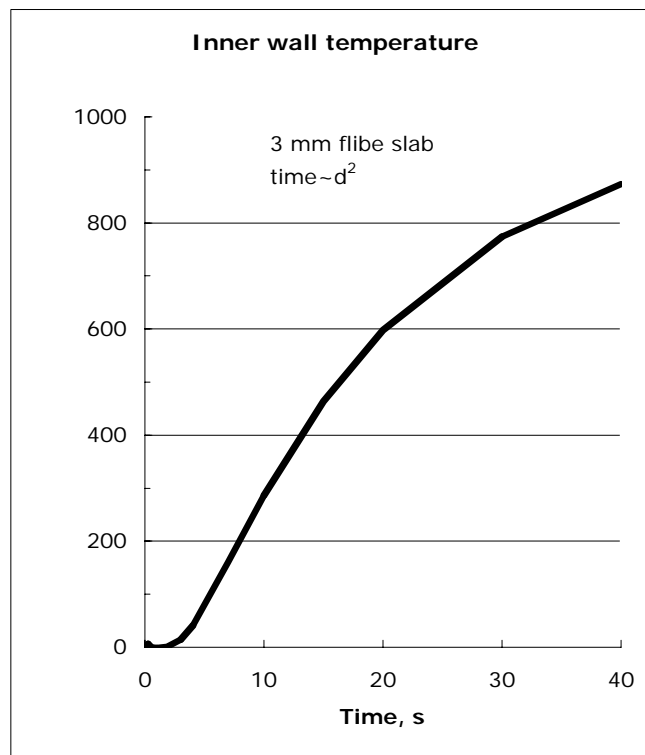
Fig. A.1.2. A carbon composite mold set for both inner and outer cones for the RTL are shown. The transition electrodes are added after molding if the design calls for them.

Temperature Response During Insertion

The temperature in the wall as a function of distance x from the center of the wall is given below:

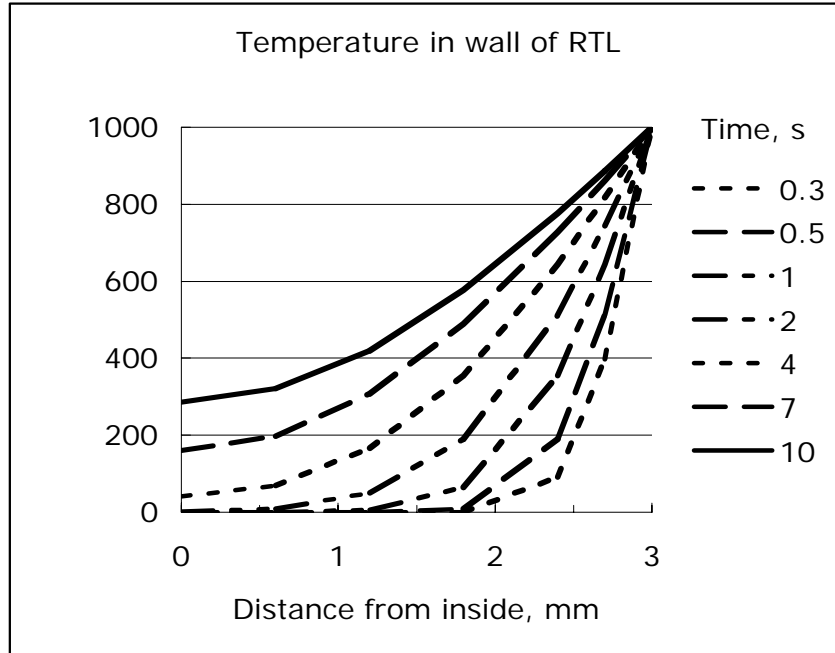
$$\frac{T_i - T}{T_i - T_f} = \frac{0 - T}{0 - 1000} = \frac{T}{1000^\circ \text{C}} = 1 - \frac{4}{\pi} \sum_{n=0}^{\infty} \frac{(-1)^n}{(2n+1)} \cos\left(\frac{(2n+1)\pi x}{2l}\right) e^{-\frac{(2n+1)^2 \pi^2 \alpha t}{4l^2}}$$

Results are shown in Figs. A.1.3 and A.1.4. For a 3 mm wall heated from one side, $l = 3$ mm. The inner surface is located at $x = 0$ mm and the outer surface being heated by condensing vapor is at $x = 3$ mm. These plots are not accurate enough for our purposes for times less than 0.3 s with only 10 terms in the equation above so the analysis in the next section is recommended for use. However, at 0.3 s and at 2.7 mm (0.3 mm from outer surface), Fig. A.1.4 shows 400 °C as does Fig. A.1.5.



(a)

Fig. A.1.3. Surface temperature versus time



(b)

Fig. A.1.4. The temperature throughout 3 mm flibe RTL wall. The relevant plot is the temperature near the outer surface (near 3 mm) for times of about 0.2 s.

Thermal Shock to Cone on Insertion

When the RTL is inserted during a time of about 0.2 s (2 m long RTL/10 m/s=0.2 s), the hot vapor quickly forms a thin film of liquid salt at or near the vapor temperature of 1000°C. This film itself forms a thermal resistance. The interior slowly heats up with a strong temperature gradient. This can cause cracking. Analysis and experiments are needed. We can calculate thermal stress from the above space and time dependent formula for temperature. The formulation of the salt can be varied to help avoid cracking by varying the ratio of LiF to BeF₂ or even adding NaF.

The temperature near the surface of the RTL during insertion is:

$$T = 1000 \text{ } ^\circ\text{C} \cdot \text{ERF}\left(\frac{x}{2\sqrt{\alpha t}}\right) \approx 1000 \text{ } ^\circ\text{C} \cdot \left(1 - \frac{x}{\sqrt{\pi \alpha t}}\right)$$

The temperature near the surface is shown below:

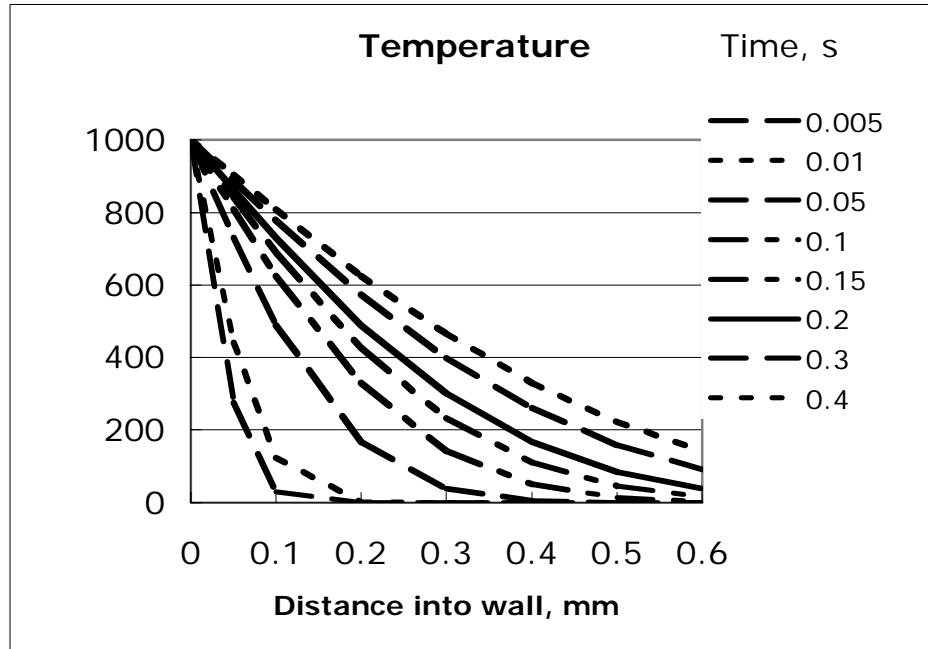


Fig. A.1.5. The surface temperature quickly jumps up to the vapor temperature and decreases inside the solid RTL material. The temperature variation will cause a stress in the frozen salt.

The coefficient of thermal expansion for solid flibe is, $\alpha = 73 \times 10^{-6} \text{ cm/cm-}^\circ\text{C}$ based on $\rho = 2.1685 - 2.2 \times 10^{-4} (T - 25^\circ\text{C})$ from Ref. [2]. The coefficient of thermal expansion for carbon composite 4-D weave is $\alpha = 0.5 \times 10^{-6} \text{ cm/cm }^\circ\text{C}$ [3], which will be useful for analysis of the mold. This value seems awfully low! Copper is $19 \times 10^{-6} \text{ cm/cm }^\circ\text{C}$ at 700 K and graphite is $9.7 \times 10^{-6} \text{ cm/cm }^\circ\text{C}$ at 700 K [4].

Mass of RTL

A simple calculation of the mass of the RTL is shown in Fig. A.1.2 above for 3 mm wall thickness average gives 75 kg for each and 400 kg for the flibe shielding bucket.

Stress During Casting

A 0.5 m radius mold made of carbon composites will shrink by $0.5 \text{ m} \times 73 \times 10^{-6} \times 480 \text{ K} = 17.5 \text{ mm}$ assuming the mold is at 20°C and the flibe poured in at 500°C . The mold is stiff and has little temperature change. This contraction will have to be dealt with.

Stress During Insertion

During insertion the hot vapor rapidly heats the surface of the cold flibe RTL. Based on LiF data, the order of magnitude of the peak stress is

$$\sigma \sim \frac{\alpha E \Delta T}{(1-\nu)2} = \frac{73 \times 10^{-6} 65 \times 10^9 \text{ Pa} \Delta T}{(1-0.33)2} = 3.5 \text{ MPa} \times \Delta T$$

where ΔT is the front to back temperature change. From Fig. A.1.5 we see the temperature drop at 10 ms is $\sim 300^\circ\text{C}$ (ignore temperature above the melting point and above the elastic-plastic transition temperature of about 300°C) in a distance of 0.04 mm giving a peak compressive stress of 2 GPa. Some failure mechanism will limit this large compressive stress. The tensile stress over the remaining 2.9 mm must balance the average compressive stress, which is 1 GPa to be compared to the apparent elastic limit of 11 MPa. The average tensile stress is $500\text{ MPa} \times 0.04\text{ mm}/(3\text{ mm}-0.04\text{ mm})=13\text{ MPa}$. This tensile stress is an over estimate due to the relaxation of the over stressed thin compressive layer. Nevertheless, the results using this rough method to calculate tensile stress are shown in Fig. A.1.6.

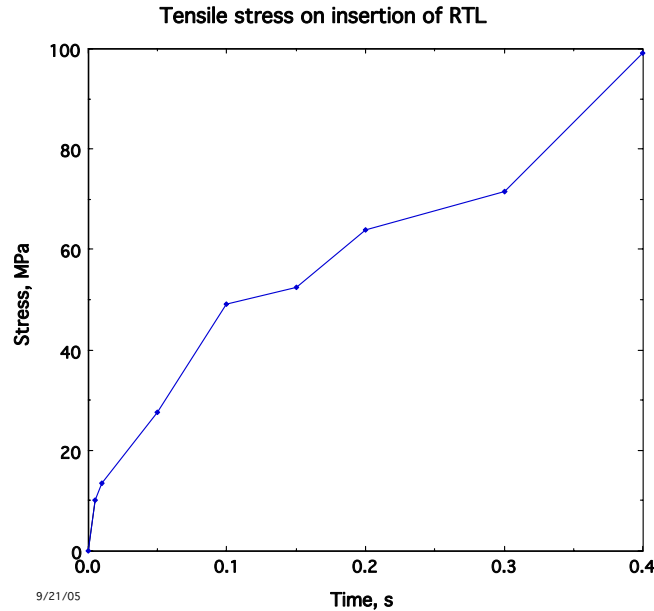


Fig. A.1.6. Tensile stress in the interior of the RTL

Unless there is some stress relieving mechanism, failure seems assured. One mechanism is plastic flow and another is cracking in the thin compressive layer that will relieve the tensile stress in the unheated interior. Some surface modification might be effective. Another idea is keep the temperature of the RTL high enough where plastic flow will relieve the thermal stress but low enough that it will maintain its shape. Experimentation and more analyses are called for.

Research Issues for Future Study

Key research issues for the flibe RTL include dealing with high stress during insertion, conducting coatings if needed such as Li, Sn, Hg, and Pb, and compatibility with baseline design.

References for Appendix A.1

- [1] Carslaw and Jaeger, Conduction of heat in solids, Second Edition Clarendon Press, Oxford(1959) p100.
- [2] R. W. Moir et al., "HYLIFE-II Progress Report," UCID-21816, p.6-13 (Dec. 1991).
- [3] W.R. Meier et al, Osiris and SOMBRERO Inertial Fusion Power Plant Designs, p. 3-34 (1992), <http://aries.ucsd.edu/LIB/REPORT/OTHER/OSIRISOMBRERO/>
- [4] Physics Handbook, p 4-66.

Appendix A.2

Tritium Inventory in Z-IFE Carbon Composite Chamber Walls

There is considerable known about tritium holdup in graphite from work in Tokamak Fusion Test Reactor (TFTR) and other devices and from the Sombrero study that used carbon composites as a chamber material. The conclusions are that there are two mechanisms for tritium hold up: 1) solubility in a graphite matrix and 2) trapping at damage sites in carbon fibers or pyrocarbon form. The soluble tritium inventory will be shown to be low, measured in mg but the inventory in damaged carbon can be < 0.1 kg or >1 kg and is strongly design dependent as will be discussed.

Tritium Inventory Due to Solubility

Causey [1] say an alternative chamber configuration that eliminates the pool at the bottom s holdup due to solubility is small in pyrographite but in regular graphite and C/C it is $S \times P^{1/2} \times$ volume. S is solubility, P is pressure.

$$S = 6.44 \times 10^{-5} e^{\frac{0.2eV}{kT}} \text{ (atom fraction / atm}^{1/2}\text{)}$$

$$T = 1000 \text{ }^\circ\text{C} = 0.116 \text{ eV}$$

$$SP^{0.5} = 3.6 \times 10^{-4} P^{0.5} \text{ atom fraction}$$

What is the Hydrogen Pressure in the Chamber?

HYLIFE-II had 1.8 mg of T₂ in its target for 350 MJ yield at 6 Hz for 1 GWe. Suppose Z has 3 GJ and a pulse rate of 6 Hz \times 0.350 GJ/3.0 GJ = 0.7 Hz for the same power.

HYLIFE-II	Z-IFE	Flow rate
1.8 mg T ₂	15.4 mg T ₂	10.8 mg/s T ₂
1.2 mg D ₂	10.3 mg D ₂	7.2 mg/s D ₂
	0.3 g H ₂	0.21 g/s H ₂

Each Z target has two liquid hydrogen reservoirs to maintain cooling totaling about 3 cm³ or about 0.3 g of H₂. The pumping and isotopic separation system will be much more involved with this large extra load of hydrogen.

Suppose we install four ducts for pumping each of 1 m² cross section with chevrons for heat shields that cut the effective pumping area of the cryogenic pumps behind by a factor of 1/3. Then the pumping speed, S', for hydrogen is

$$S' = A\bar{v} / 4 = \frac{4m^2}{3} \frac{2200m^2}{4} \sqrt{\frac{1273}{2 \cdot 300}} = 1068m^3 / s = \text{millionliter} / s$$

$$n = Q/S' = 0.21 \text{ g/s H}_2 / 1068 \text{ m}^3/\text{s} = 1.97 \times 10^{-4} \text{ g of H}_2/\text{m}^3$$

$$= 1.97 \times 10^{-4} \text{ g/m}^3 / 2 \times 1.67 \times 10^{-27} \text{ kg/H} = 5.89 \times 10^{19} \text{ H}_2/\text{m}^3 = 2.7 \text{ mTorr of H}_2$$

$$5.89 \times 10^{19} \text{ H}_2/\text{m}^3 \times 10.8 \text{ mg/s T}_2/3 \times 0.21 \text{ g/s H}_2 = 1.0 \times 10^{18} \text{ T}_2/\text{m}^3 = 1.0 \times 10^{18} \text{ D}_2/\text{m}^3 = 45 \text{ } \mu\text{Torr}$$

At 1000 °C, $2.2 \times 10^{22}/\text{m}^3/\text{Torr}$

$$SP^{0.5} = 3.6 \times 10^{-4} \times \left(\frac{2.7 \times 10^{-3} \text{ Torr}}{760 \text{ Torr}} \right)^{0.5} = 6.8 \times 10^{-7} \text{ atom fraction of H}_2$$

The hydrogen dilutes the tritium by the ratio of $4.6 \text{ } \mu\text{Torr}/2.7 \text{ mTorr} = 0.017$. So the tritium dissolved is $6.8 \times 10^{-7} \times 0.017 = 1.2 \times 10^{-8}$ atom fraction of T_2 . Each m^3 of carbon component at 1500 kg/m^3 contains

$$1.2 \times 10^{-8} \times 1500 \text{ kg/m}^3 \times \frac{3 \text{ amu}}{12 \text{ amu}} = 4.3 \text{ mg/m}^3$$

Suppose the chamber has 500 m^2 of area exposed to the tritium gas. Also, suppose there is a SiC layer 1 to 10 mm into the C/C as shown in Fig. A.2.1. Then there is 0.5 to 5 m^3 of C/C exposed to tritium to be dissolved. The amount of tritium for 1 mm layer of C/C is 2 mg and for a 10 mm layer is 20 mg.

This is an underestimate due to the flibe passages in the walls and piping and heat exchanger walls. The key assumptions to keep an eye on are: wall area $\approx 5 \text{ m}^2$, SiC layer 10 mm into C/C composite, hydrogen pressure $\sim 2.7 \text{ mTorr}$, tritium pressure = $45 \text{ } \mu\text{Torr}$.

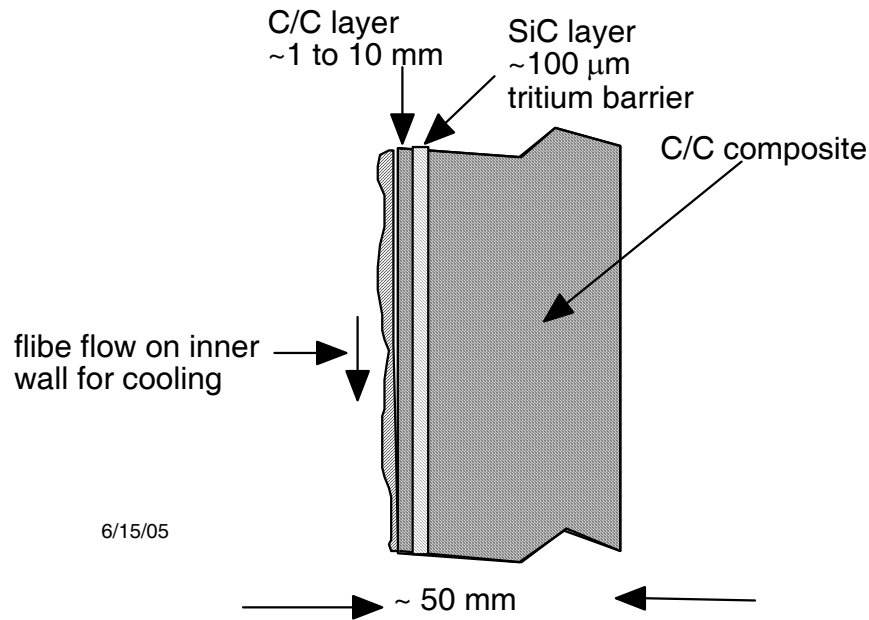


Fig. A.2.1. Carbon composite chamber wall with a SiC tritium barrier embedded in the composite.

Tritium Inventory Due to Trapping at Damage Sites

Causey [2] discusses a second mechanism for tritium inventory in graphite in addition to solubility and that is trapping. After only a little neutron irradiation of about 0.01 dpa, trapping sites are produced that hold tritium with 4.3 eV binding energy. A plausible explanation is previously bonded carbon by dislocations find themselves with free bonds available to take up tritium as it arrives. This effect saturates at an inventory of about 1000 appm for irradiation exceeding 0.1 dpa. Simply stated, we can expect tritium to build up to this level in addition to the solubility amount. Of course, any isotope of hydrogen will take up these sites, so isotopic dilution must be accounted for.

$1500 \text{ kg carbon}/\text{m}^3 \times 1000 \times 10^{-6} = 1.5 \text{ kg carbon}/\text{m}^3$ that have hydrogen attached in saturation. To get the inventory of tritium we need the volume of carbon exposed (0.5 to 5 m^3) and the fraction of hydrogen that is tritium $\frac{10.8 \text{ mg } T_2}{0.21 \text{ g } H_2} \cdot \frac{1}{3} = 0.017 \text{ T/H atom ratio}$

Tritium inventory = $1.5 \text{ kg carbon}/\text{m}^3 \times 0.5 \text{ m}^3 \times 0.017 \text{ T/H atom ratio} \times \frac{3 \text{ g } T}{12 \text{ g } C} = 3.2 \text{ g } T$ and

for the 5 m^3 case 32 g . If we do away with the liquid hydrogen reservoir, then the tritium inventory is $1.5 \text{ kg carbon}/\text{m}^3 \times 0.5 \text{ m}^3 \times 0.5 \text{ T}/(1D+1T) \times \frac{3 \text{ g } T}{12 \text{ g } C} = 94 \text{ g } T$ for the 1 mm case

and 940 g for the 10 mm case.

Conclusion

With a silicon carbide layer 10 mm into the carbon composite wall that prevents exposure of the bulk of the material to tritium buildup, we calculate a 20 mg tritium inventory due to solubility and a 32 g inventory due to the trapping mechanism after modest irradiation of only 0.1 dpa. If the SC layer were not used this number would increase by a factor of about 5 for a 50 mm thick wall. One reason the inventory is so low is the almost a factor of 100 isotopic dilution of tritium by hydrogen due to the liquid hydrogen reservoir included in each target. This will add greatly to the pumping and isotopic separation system. If the liquid hydrogen reservoir is eliminated, the tritium inventory goes up to 94 g for the 1 mm layer case and 940 g for the 10 mm case.

References for A.2

- [1] R. A. Causey, "The interaction of tritium with graphite and its impact on tokamak operations," *J. Nuclear materials* **162-164** (1989) 151-161.
- [2] R. A. Causey, K. L. Wilson, W. R. Wampler, B. L. Doyle, "The effects of neutron irradiation on the trapping of tritium in graphite," *Fusion Technol.*, **19** (1991) 1585-1588.

Appendix A.3

Flibe Vapor Pressure and Evaporation (Condensation) Rates

The vapor pressure and evaporation rates are calculated from the following equations and plotted in Fig. A.3.1 and A.3.2:

$$P(\text{Pa}) = e^{A-B/T}$$

$$J = \frac{n\bar{v}}{4} = \frac{p}{(2\pi mkT)^{0.5}} = CT^{-0.5} e^{(A-B/T)}$$

Here, $A=26.59$, $B=25,390$ and $C=3.828 \times 10^{23}$ for BeF_2 evaporation. The flibe vapor pressure used was $\log_{10} P_{\text{torr}} = 9.424 - 11026.208/T(\text{K})$ [1,2] and was converted to pascals. At equilibrium $J_{\text{evaporation}} = J_{\text{condensation}}$ as shown in Fig A.3.3. The significance of the condensation rate will be found when considering the fill rate of gaps near the target in the RTL. Another important consideration is the vapor leak rate during insertion. For most cases the RTL surface can be considered to be coated with flibe at the vapor temperature and immediately begin to evaporate at the same rate as the condensation.

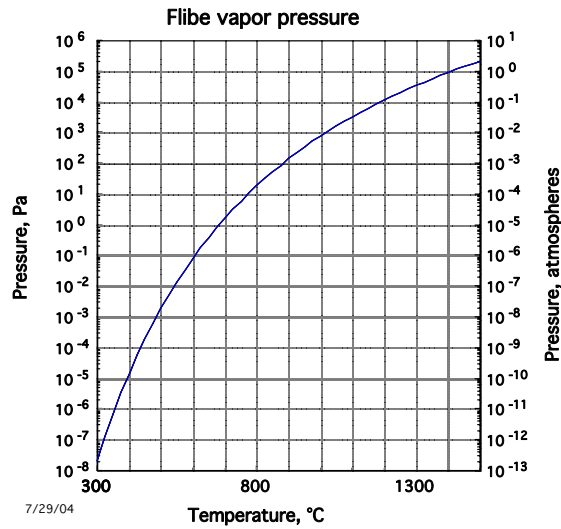


Fig. A.3.1. Vapor pressure for flibe. To convert to units of Torr use $P(\text{Torr}) = P(\text{Pa})/133.3$.

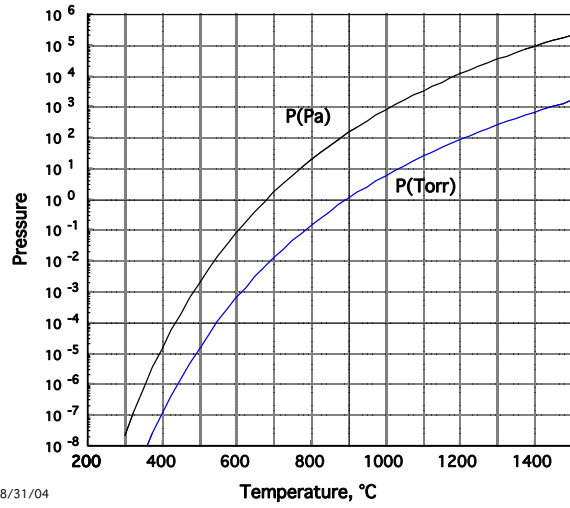


Fig. A.3.2. Flibe vapor pressure in Pa and Torr.

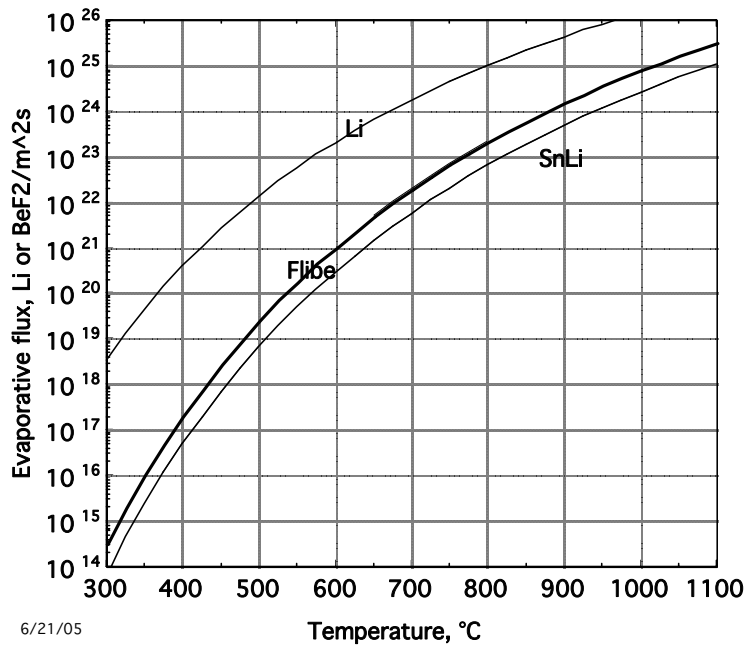


Fig. A.3.3. Evaporation (and condensation) rates into vacuum for candidate liquids.

Appendix A.4

Flibe Processing

The molten salt, flibe, in the Z-IFE will have to be processed to remove target material and contaminants from leaks and corrosion products. This subject has been discussed in a previous report on HYLIFE-II processing from which much of the present discussion is taken [3]. The processing system envisioned is shown in Fig. A.4.1. There must be provision to remove volatiles and that is shown in Fig. A.4.2 and for solids or liquid precipitates and those are shown in Fig. A.4.3.

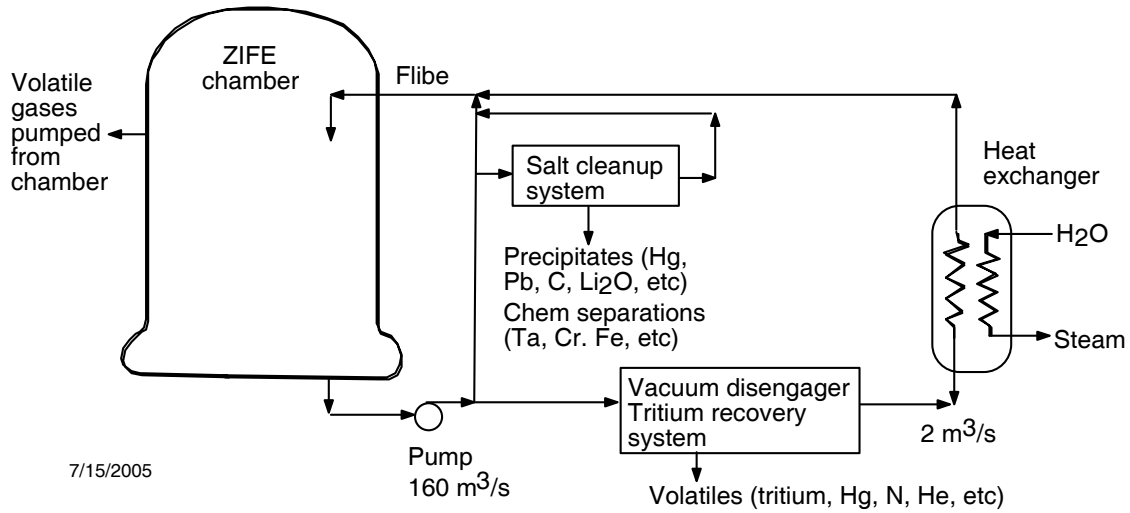


Fig. A.4.1. Molten salt processing system for IFE.

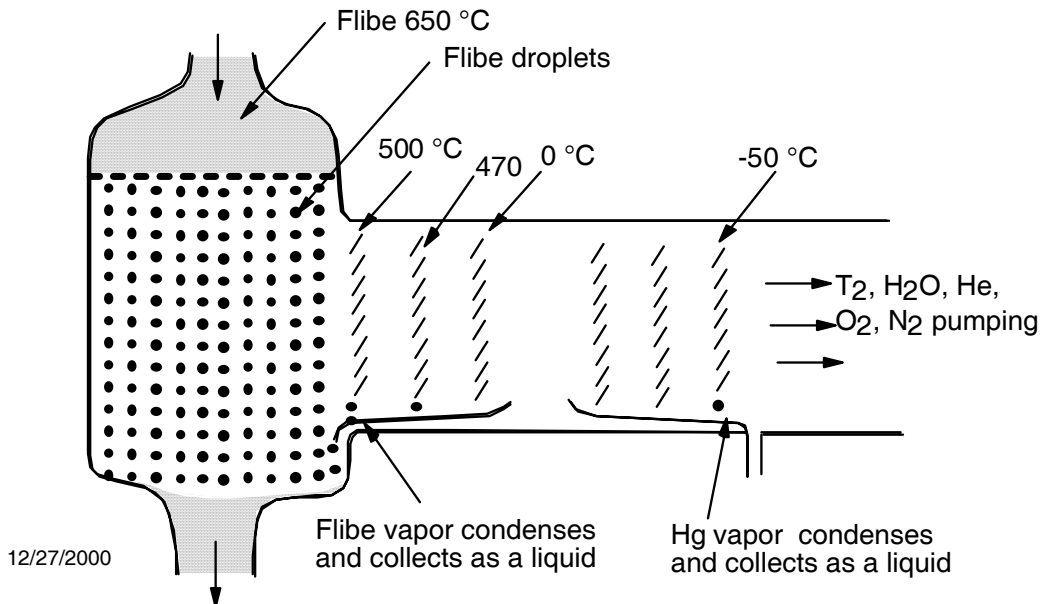


Fig. A.4.2. Vacuum disengager modified to remove mercury vapor and other volatile materials from flibe.

The vacuum disengager was designed to handle 10,000 L/s flibe processing rate for HYLIFE-II, which was the full flow to the heat exchangers. The cost was considerable and a lesser processing rate would be desirable. For Z-IFE with a 200 K temperature across the heat exchanger rather than 50 K for HYLIFE-II, the flow rate is four times lower or 2,000 L/s.

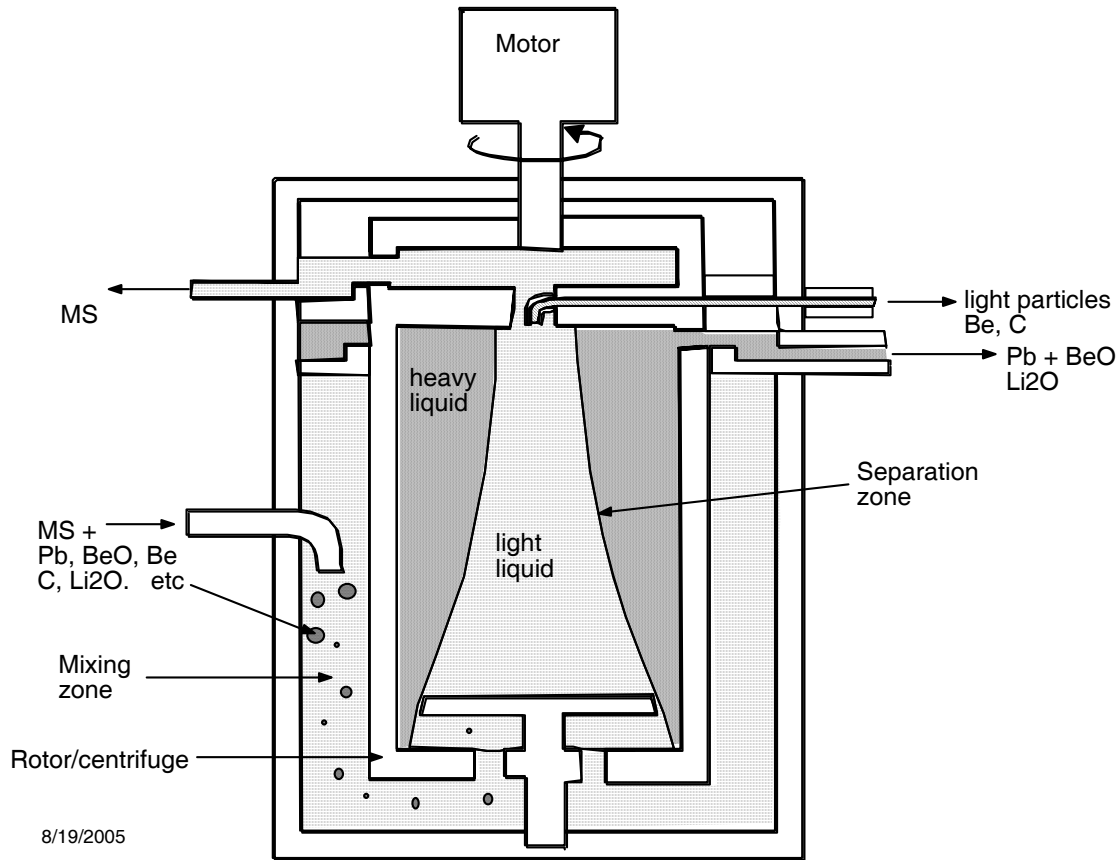


Fig. A.4.3. Schematic illustration of a centrifugal separator design from a working ANL cadmium-chloride salt contactor (Chow et al. [4,5]).

The centrifuge shown in Fig. A.4.3 had a 4-cm-diameter rotor and operated at ~ 1 L/min. We assume it can be scaled up in diameter to 25 cm based on operating experience with aqueous/organic separators and have a process throughput rate of 2 L/s. Then five units would give 10 L/s processing rate.

Process Rates

We will assume [6] each shot or each target will have the materials to be removed shown in Table A.4.1. For high-Z material, we take 3 g from p. 778 of SNL's FY04 report. We will further assume a 1 Hz pulse rate so that these numbers become the processing rate required. These numbers are considered nominal. If the amount of any element such as C were 5 mg rather than 1 mg then the results of the calculations would be scaled by a factor of five. Similarly the results

can easily be scaled with pulse rate and other parameters. We will not discuss the removal of D and T and H here as that is well discussed elsewhere and is a standard problem, however, this is not to understate the cost of such processing. The beryllium comes from the target capsule.

From a processing point of view it would be desirable to find a substitute for beryllium. The beryllium ($\rho=1.8 \text{ g/cm}^3$) being lighter than flibe ($\rho=2 \text{ g/cm}^3$) would come out of the centrifuge with the light stream and then sent to the off-line hydro-fluorinator ($\text{HF}+\text{H}_2$) where it is turned into BeF_2 and returned to the molten salt. We could add two moles of HF to the target for each mole of beryllium in the target. This is essentially an in situ hydro-fluorinator. Water and air leaks will result in O. The O will come out as Li_2O ($\rho=2 \text{ g/cm}^3$) and together with the BeO ($\rho=3 \text{ g/cm}^3$) will come out with the heavy liquid from the centrifuge unless it is soluble in which case it will be removed in the hydro-fluorinator. These also will go to the hydro-fluorinator for removal. The C ($\rho=2 \text{ g/cm}^3$) and Be ($\rho=1.8 \text{ g/cm}^3$) will be centrifuged and filtered. C and Li_2O are both have densities close to flibe so separation might not be easy.

This leaves the high-Z material to discuss. Target designers and fabricators like to use Au. Studies show gold is affordable (\$30 M as shown later) in a power plant with a high process rate but somewhat costly as discussed in Ref 1 and not recommended. We recommend looking at three alternatives for high-Z materials: Hg, Pb, and W. These elements are used for the wires and the hohlraum walls. Hg would have to be kept cold, likely about -100 C. Its volatility means it would be recovered along with other gasses such a tritium with high process rates and low inventories (~wppm). Lead would precipitate and be removed in the centrifuge and be left at the ~170 wppm level at a process rate of 10 L/s as will be discussed next. W would precipitate and could be removed by centrifuging and filtration. We could imagine fluorination (F_2) of tungsten for removal to avoid filtering or to augment filtering but this is a very corrosive process. The FY2004 report, page 785 discusses removal of W by reacting with C and growing a WC solid ($\rho = 17 \text{ g/cm}^3$).

Table A.4.1 Materials per shot

DT	25 mg
Be	150 mg
High-Z	3 g
C	1 mg
O	1 mg

The contaminant fraction of material left in the flibe after processing, f is

$$f = \frac{\text{masscontaminant}}{\text{massflibe}} = \frac{S}{\dot{V} \cdot \eta \cdot \rho_{\text{flibe}}}$$

S = input rate (kg/s)=0.003 kg/s

\dot{V} = process rate (m^3/s) = 10 L/s = 0.01 m^3/s

V = volume of flibe = 2000 m^3

η = fraction removal per pass = 0.9

ρ_{flibe} = density of flibe = 2000 kg/m^3

For the nominal numbers, $f=1.7 \times 10^{-4} = 170$ wppm
 The average residence time or hold up of material is

$$t = \frac{V}{\dot{V} \cdot \eta} = 2.2 \times 10^5 \text{ s} = 2.6 \text{ days}$$

The inventory is

$$M = \frac{V \cdot S}{\dot{V} \cdot \eta} = 6.7 \times 10^5 \text{ g} = 670 \text{ kg}$$

This is \$9M at \$400/oz if it were gold.

Table A.4.2
 Process rates

Process rate liters/s	Time to process total inventory	Inventory	
		kg	wppm High-Z/flibe
10,000	120 s (3.7 min)	0.67	0.17
1,000	2.2×10^3 s (37 min)	6.7	1.7
100	2.2×10^4 s (6.1 hrs)	67	17
10	2.2×10^5 s (2.6 days)	670	170
1	2.2×10^6 s (26 days)	6,700	1,700

Because the high process rate equipment is already installed to remove the volatile tritium, mercury could be processed at a rate over 1,000 L/s for a contamination level of less than 1.7 wppm and an inventory of 6.7 kg. Lead or tungsten would be processed at a rate of 10 L/s with a 2.6-day inventory, 170 wppm or 670 kg. Corrosion studies should consider lead at 170 wppm or mercury at ~1 wppm.

From a processing point of view, mercury is preferred. Next preferred is lead. Tungsten is the most difficult from a processing point of view.

References for Appendix A.4

- [1] D. R. Olander, G. T. Fukuda, and C. F. Baes, Jr., "Equilibrium pressure over BeF₂/LiF (Flibe) molten mixtures," *Fusion Technology*, **41**, 141 (2002).
- [2] M. R. Zaghloul, D. D. Sze and A. R. Raffray, "Thermo-physical properties and equilibrium vapor-composition of lithium fluoride-beryllium fluoride (2LiF/BeF₂) molten salt," *Fusion Science and Technology*, **44**, 344-350 (2003).
- [3] R. W. Moir, "Flibe coolant cleanup and processing in the HYLIFE-II inertial fusion energy power plant," UCRL-ID-143228 (2001). www.osti.gov/servlets/purl/15006180-1kse4O/native/
- [4] L.S. Chow, J.K. Basco, J.P. Ackerman, and T.R. Johnson (1993), "Continuous extraction of molten chloride salts with liquid cadmium alloys," Global 93, Int. Conf. and Technology exhibition future nuclear systems: emerging fuel cycles and wastes disposal options, **2**, 1080-1085 (1993?).
- [5] L.S. Chow, J.K. Basco, E.L. Carls, and T.R. Johnson, "Testing of pyrochemical centrifugal contactors," DOE Spent Nuclear fuel and fissile material management embedded topical meeting, Spent nuclear fuel-treatment technologies, Reno, Nevada, June 16-20, 1996.
- [6] Rick Olson, Private communication, SNL, July 13, 2005.

Appendix A.5

Flat Plate Heat Exchanger Based on Carbon Composites with SiC Barriers

The idea is to make a heat exchanger out of flat plates of C/C composite sheets. They are stacked up as shown. The top and bottom sheet is a strong backing plate that can withstand bending and graphite bolts clamp the stack together. The improvements introduced here is to use bolts for pretension and silicon sheets and coatings to be reacted all at once in an autoclave forming SiC. The application might be IFE or MFE or fission reactors where the primary coolant is flibe containing tritium and the secondary is a non-radioactive molten salt such as $\text{NaBF}_4 + \text{NaF}$. The silicon carbide will help prevent tritium from getting to the environment. Flibe to helium is also possible.

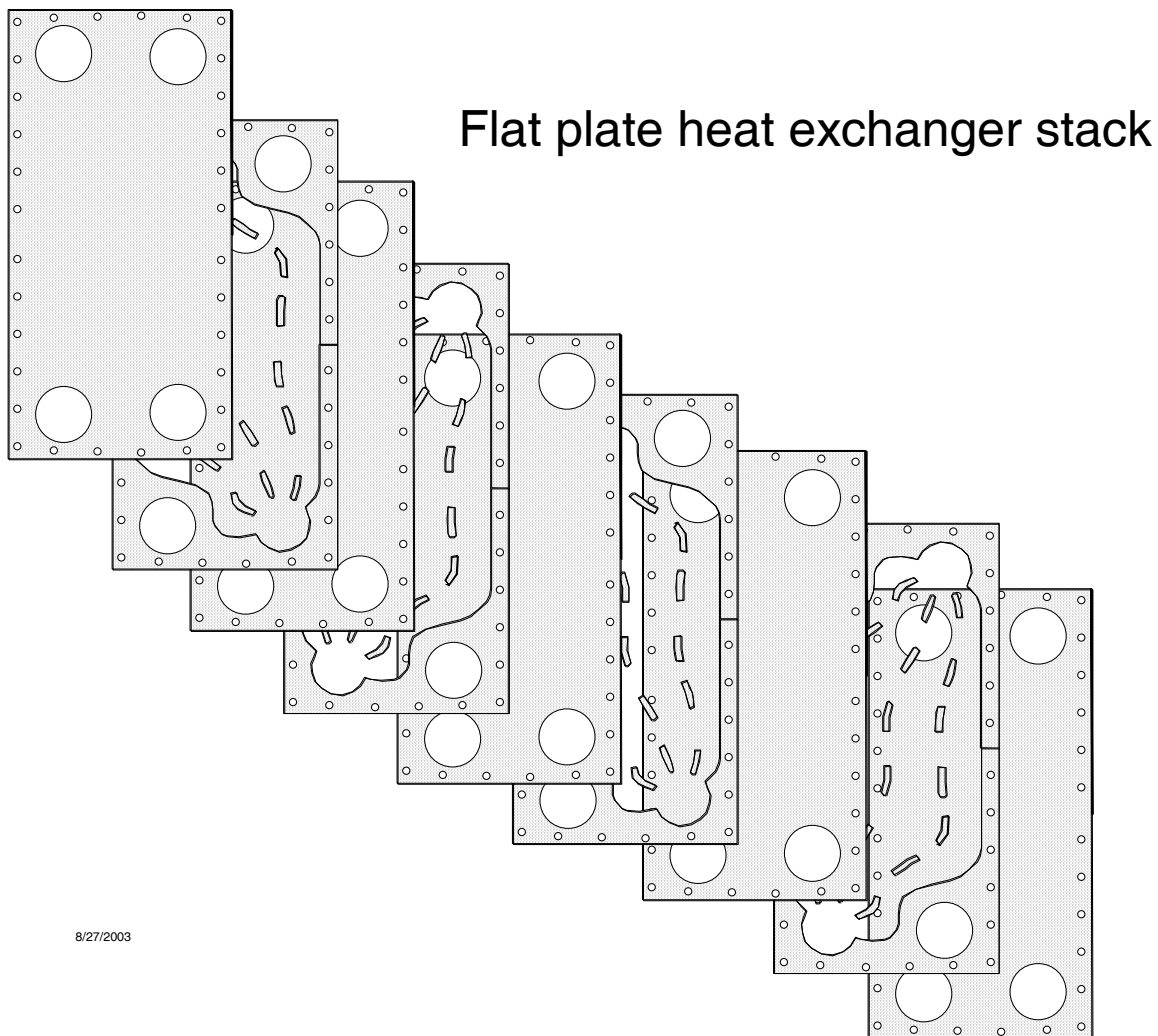


Fig. A.5.1. Flat plate heat exchanger made of stacked sheets.

A cross-section through the inlet port and the outlet port diagonally across the heat exchanger we see the flibe coolant circuit and if we then make a cut along the other diagonal shows the $\text{NaBF}_4 + \text{NaF}$ secondary coolant circuit. Other secondary coolant salts are possible.

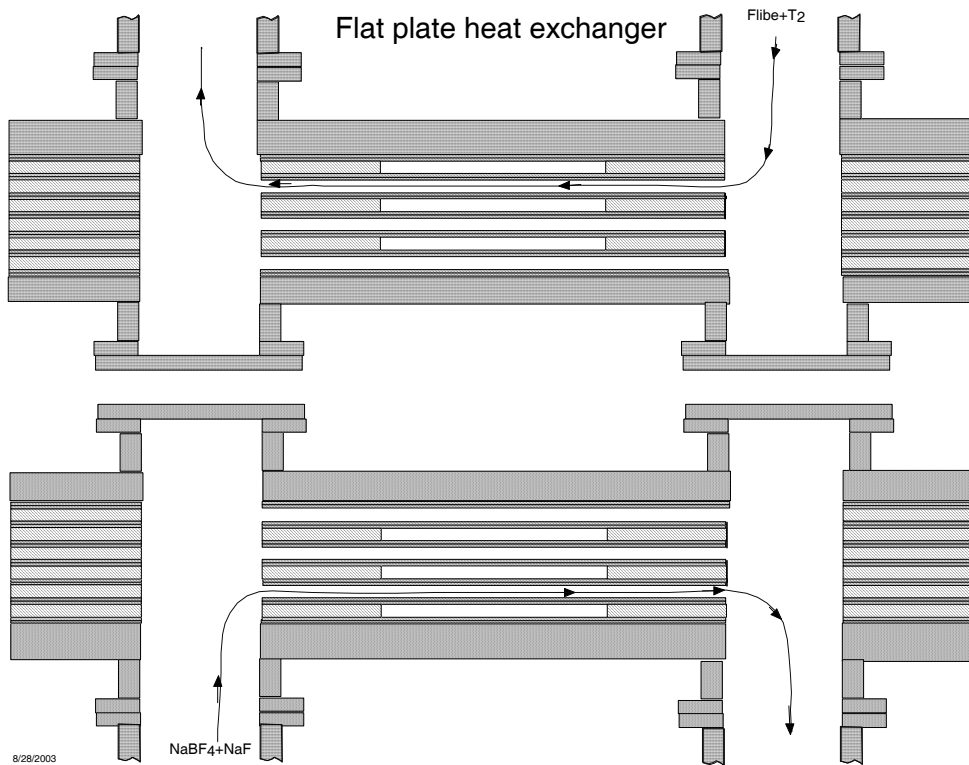


Fig. A.5.2. A cross-section through the heat exchanger diagonally from inlet and outlet ports.

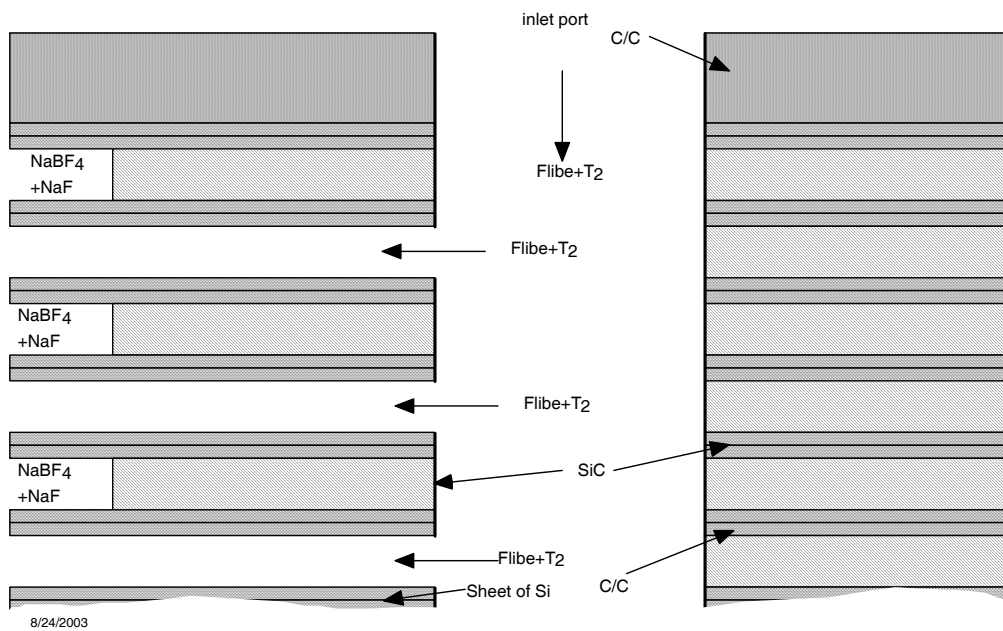


Fig. A.5.3. The region near the ports are shown in more detail.

Thin sheets of silicon (~20 μm) are sandwiched between the ~1 mm C/C sheets. Silicon is also coated on the inside of the ports. When they are fired in an autoclave the silicon reacts with the C forming SiC that is an impervious barrier to tritium. Will the SiC layers withstand differential thermal expansion? Will the barriers have cracks? SiC is known to be good barriers to tritium permeation.

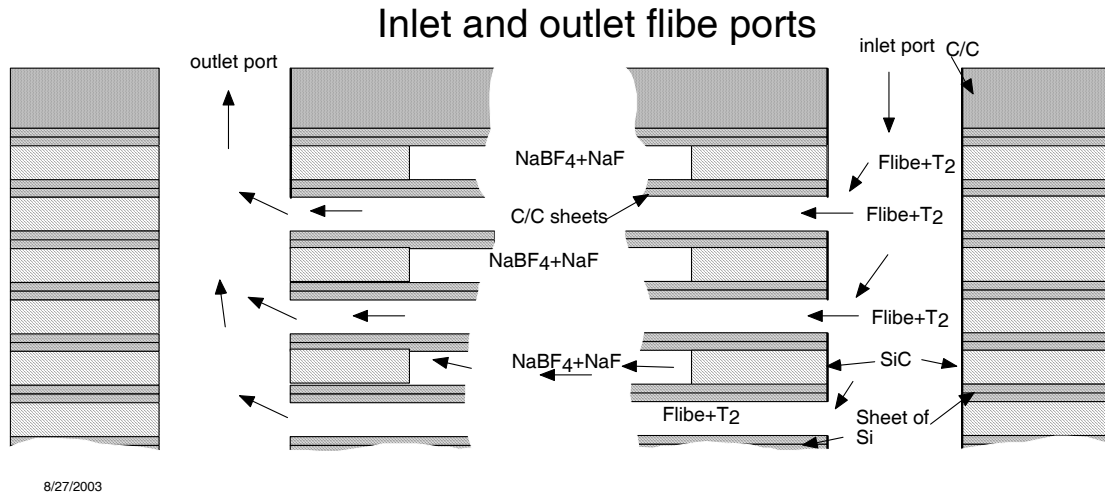


Fig. A.5.4. A cross-section from one inlet flibe port diagonally to the outlet flibe port.

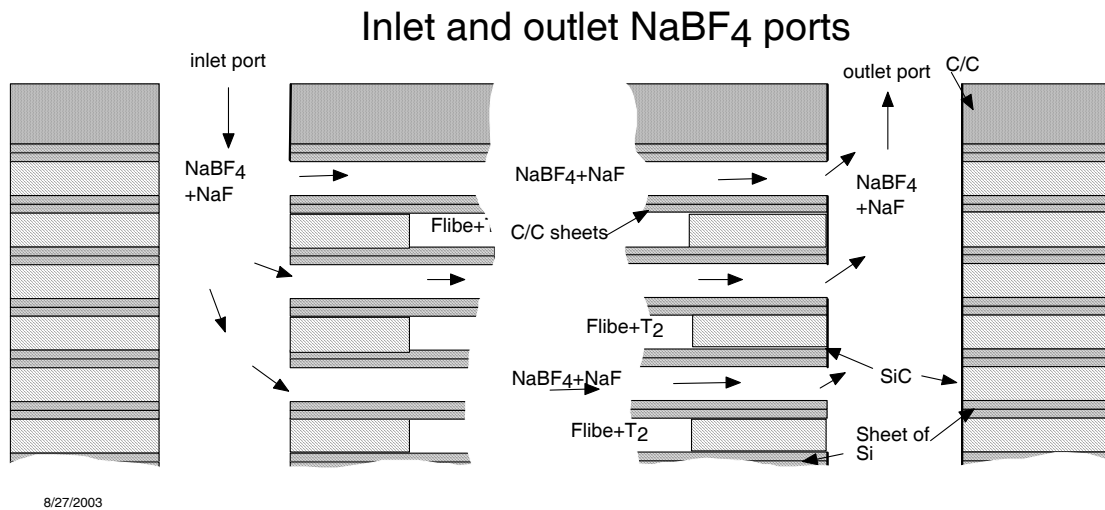
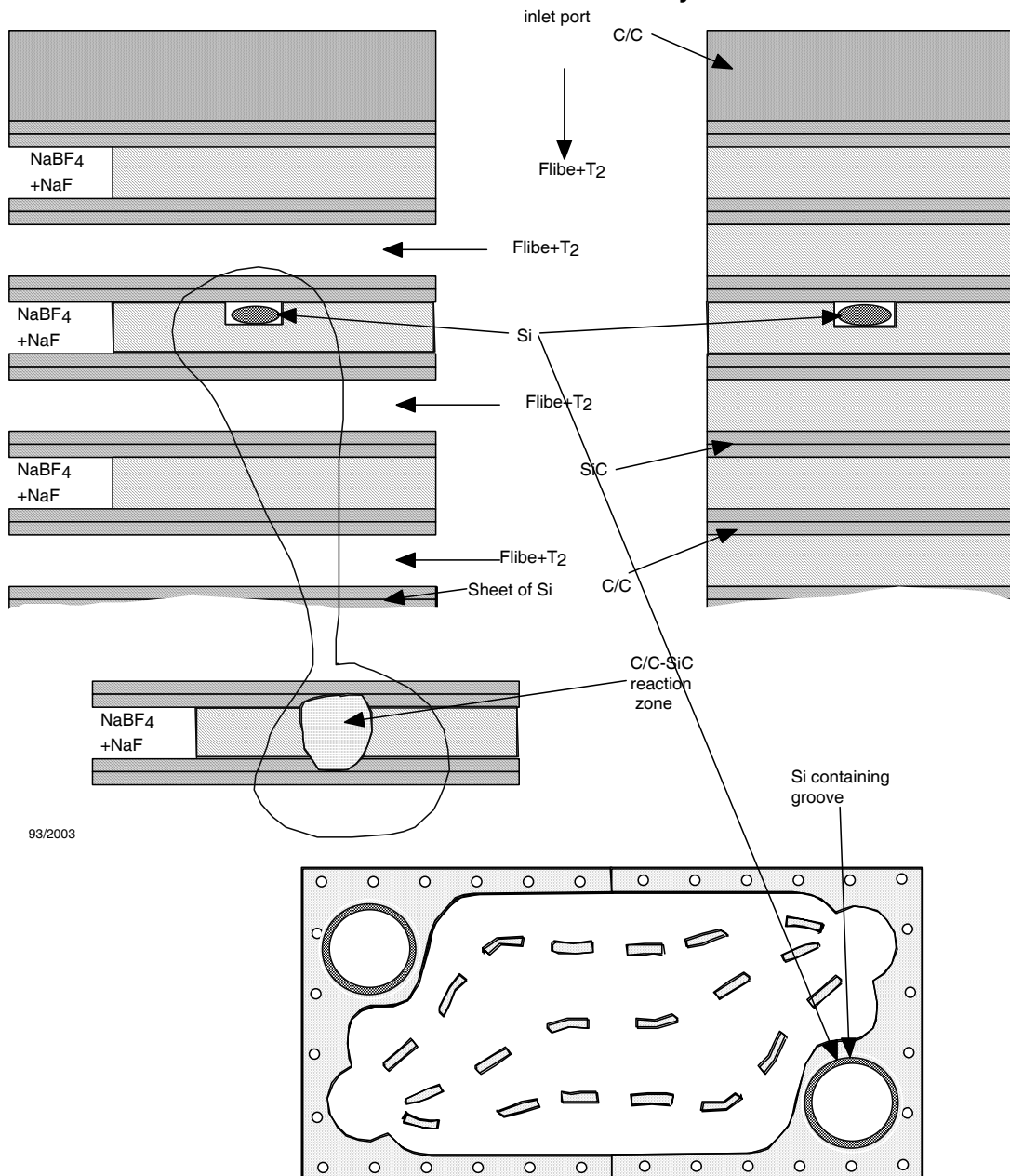


Fig. A.5.5. A cross-section from the inlet secondary molten salt (NaBF₄+NaF) port diagonally to the outlet port is shown.

A method to form a SiC barrier to tritium permeation is shown in Fig. A.5.6. The flibe that does not wet carbon will not directly contact the SiC or unreacted metallic Si. This should reduce concerns over material corrosion and transport. Also the SiC zone is embedded within the C/C composite so that cracking or debonding between the SiC and C/C regions should not lead to leaks, although clearly it would lead to tritium permeation through that crack. The question is, will the silicon migrate sufficiently and then react forming a tritium barrier.

Silicon is reacted to form a tritium permeation barrier but hidden from attack by flibe



93/2003

Fig. A.5.6. A groove is formed around an inlet and outlet port and filled with silicon. The silicon reacts forming a tritium permeation barrier of SiC.

Appendix A.6

Thermal Stress in Carbon-Carbon (C-C) First Wall

Introduction

After penetrating the liquid shielding, neutrons and gammas will be absorbed in the first-wall. They will volumetrically heat it and set up stress inducing temperature profiles that may or may not be significant to its survival. This analysis addresses the issue of thermal stresses in a carbon-carbon composite (C-C) Z-IFE first-wall for the LLNL Z-IFE baseline chamber concept.

Volumetric Heating

The transient volumetric heating from a 4.7 GJ fusion yield at the target plane of a cylindrical C-C composite first-wall with a radius of 6 m and a thickness of 0.1 m was calculated with the TART code [1]. A flibe curtain of jets from $r = 1$ m to 4 m with a packing of 33% attenuated neutrons before they hit the first wall. Table A.6.1 shows the results of this calculation. The first row is position (m) and the first column is time (s). All other entries are corresponding volumetric heating in W/m^3 . The total volumetric energy deposition in the wall is $1.45E5 J/m^3$.

Table A.6.1. The volumetric heating of 6-m-radius, 0.1-m-thick cylindrical C-C composite first-wall with a 4.7 GJ yield.

t (s) / x (m)	5.0E-03	1.5E-02	2.5E-02	3.5E-02	4.5E-02	5.5E-02	6.5E-02	7.5E-02	8.5E-02	9.5E-02
2.5E-08	2.42E+11	3.08E+11	2.35E+11	2.44E+11	2.25E+11	2.01E+11	2.05E+11	1.56E+11	1.38E+11	1.36E+11
7.5E-08	1.03E+12	1.04E+12	9.72E+11	9.29E+11	8.80E+11	7.70E+11	7.23E+11	7.40E+11	5.90E+11	5.75E+11
1.5E-07	5.46E+11	5.27E+11	5.06E+11	4.76E+11	4.37E+11	4.04E+11	3.94E+11	3.44E+11	3.02E+11	2.86E+11
2.5E-07	2.68E+11	2.62E+11	2.37E+11	2.07E+11	2.07E+11	1.81E+11	1.51E+11	1.38E+11	1.27E+11	1.04E+11
3.5E-07	1.69E+11	1.56E+11	1.49E+11	1.32E+11	1.20E+11	1.06E+11	9.65E+10	8.33E+10	7.00E+10	5.46E+10
4.5E-07	1.13E+11	1.08E+11	1.01E+11	9.10E+10	8.48E+10	6.74E+10	5.93E+10	5.15E+10	4.22E+10	3.02E+10
5.5E-07	7.45E+10	7.04E+10	6.23E+10	5.59E+10	4.97E+10	4.26E+10	3.42E+10	3.08E+10	2.39E+10	1.79E+10
6.5E-07	4.66E+10	4.39E+10	3.80E+10	3.39E+10	2.95E+10	2.51E+10	2.17E+10	1.92E+10	1.47E+10	9.41E+09
7.5E-07	3.31E+10	3.19E+10	2.49E+10	2.50E+10	1.86E+10	1.58E+10	1.28E+10	1.22E+10	9.25E+09	5.92E+09
8.5E-07	2.38E+10	2.04E+10	1.82E+10	1.45E+10	1.17E+10	9.71E+09	7.88E+09	9.19E+09	5.74E+09	4.55E+09

Interpolations of this data were then used to generate a “heating file” for transient thermal conduction code the RadHeat [2]. Figure A.6.1 shows the transient temperature profiles calculated by RadHeat after the application of a large number of pulses to reach quasi steady state conditions assuming an insulated first-wall.

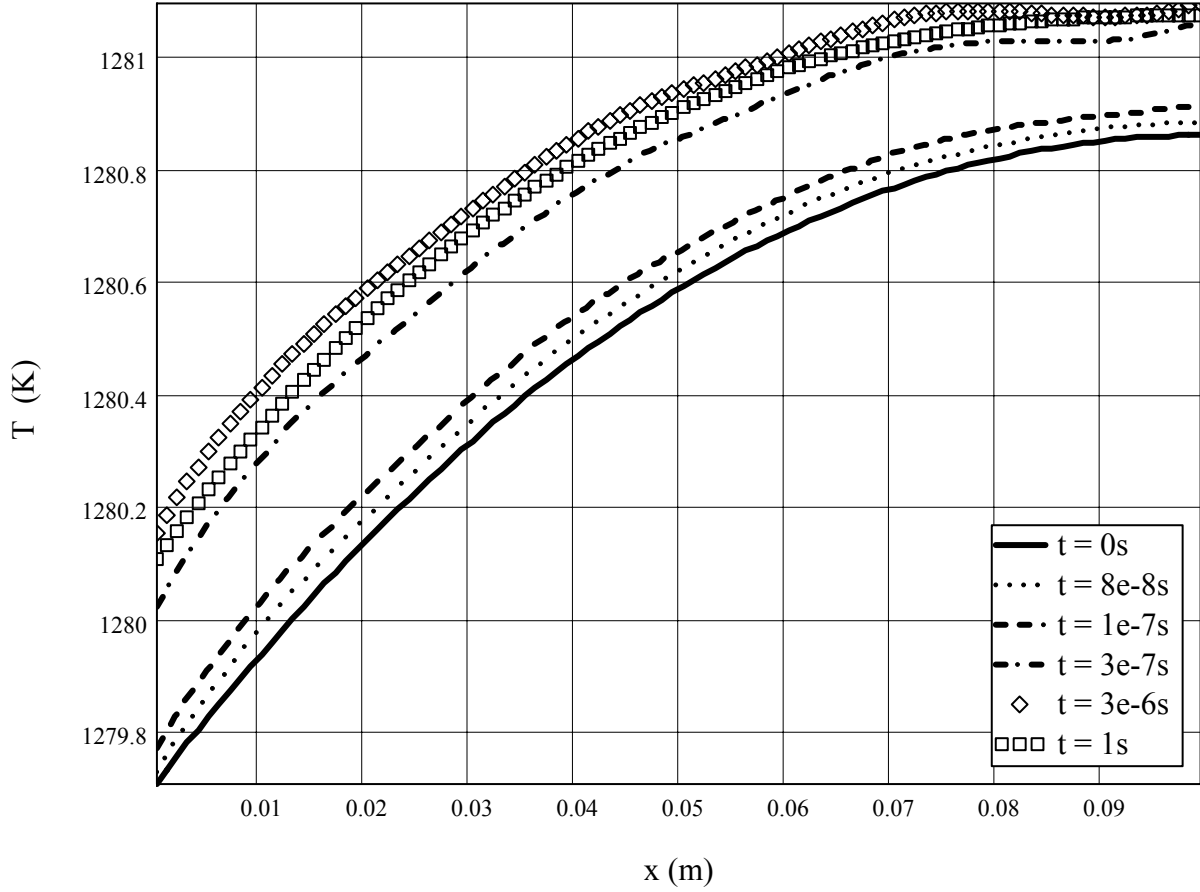


Fig. A.6.1. Temperature profiles in first-wall initially at 1273 K at various times after the application of 250 pulses to reach quasi steady state conditions.

Because neutron and gamma heating is fairly uniform throughout the first-wall, large perturbations to the steady state temperature profile (at $t = 0$ s in Fig. A.6.1) are not induced and the thermal stresses can be expected to remain constant throughout a pulse period.

The steady state data was interpolated to get a continuous function for the temperature variation in the wall. This was then substituted into the expression for the thermal hoop stress at position (r) in a cylinder that is given below [3].

$$\sigma_{\theta}(r) := \frac{E\alpha}{1-\nu} \left[\frac{1}{b^2 - a^2} \left(1 + \frac{a^2}{r^2} \right) \int_a^b \Delta T(r' - a) \cdot r' dr' + \frac{1}{r^2} \int_a^r \Delta T(r' - a) \cdot r' dr' - \Delta T(r - a) \right]$$

In this equation, E is the elastic modulus of the C-C composite, α is its thermal expansion coefficient, and ν is Poisson ratio. ΔT is the function interpolated from the RadHeat results giving the difference between the local and average temperature as a function of position. The first-wall's inner radius is a , and its outer radius is b . Figure A.6.2 shows the resulting thermal hoop stress that will be generated.

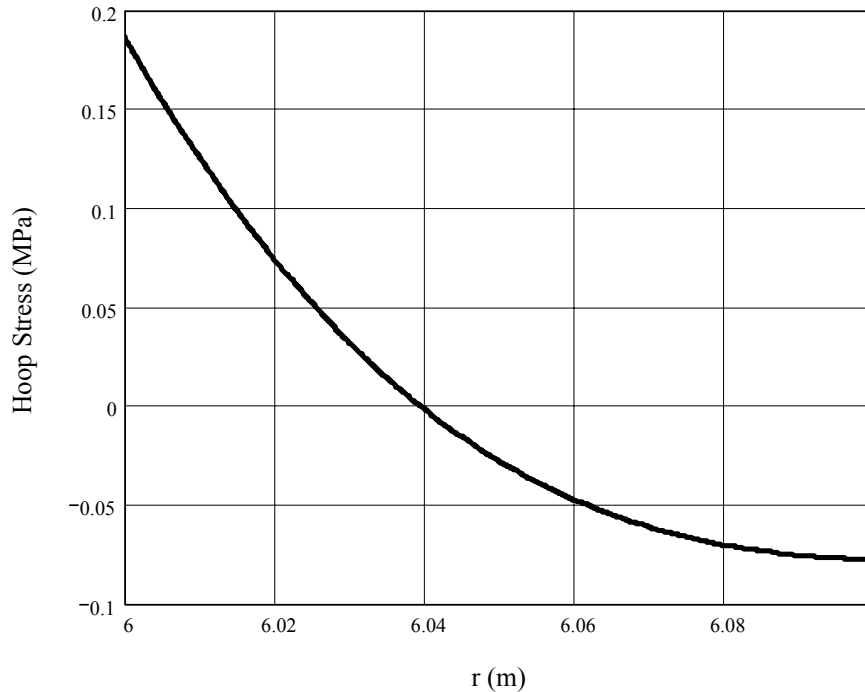


Fig. A.6.2. Thermal hoop stress in a C-C composite first-wall due to volumetric neutron and gamma heating.

As can be seen, the stresses generated are far below anything that might threaten the first-wall. Both the radial and axial (z-direction) stresses were completely negligible and ignored.

This analysis has been checked against a simpler analysis that assumes that all of the neutron and gamma energy absorbed by the first-wall is not volumetrically deposited but rather conducted from the outside surface. The linear temperature profile that results generates stresses only 20% higher than those found in this less conservative (though more accurate) analysis.

The following carbon-carbon composite material properties were used in this analysis [4]:

Elastic modulus: 55 GPa

Thermal expansion coefficient: 1.5×10^{-6}

Poisson ratio: 0.1

Thermal conductivity: 275 W / (m K)

References for Appendix A.6

- [1] D.E. Cullen, "Users Manual for TART 2002: A Coupled Neutron-Photon 3-D, Combinatorial Geometry Time Dependent Monte Carlo Transport Code," UCRL-ID-126455-REV-4, 2003.
- [2] R. P. Abbott, "RadHeat V1 User's Manual," UCRL-SM-208820, 2005.
- [3] Z. Zudans, T.C. Yen, and W.H. Steigelmann, Thermal Stress Techniques in the Nuclear Industry, New York, New York: Elsevier, p. 234, **1965**.
- [4] http://www.goodfellow.com/csp/active/static/A/Carbon-Carbon_Composite.HTML